University of Glasgow

VIA VERITAS VITA

Industrial Project EE5

January 2012

Modelling and Analysis of the Electrical and Thermal Transients following the Quench of a Superconducting Electromagnetic Coil within the Large Hadron Collider's Inner Triplet System.

Scott M. Rowan

0506704

Submitted in fulfilment of the requirements for the

Degree of Master of Engineering

Research and Project work completed at the

European Organization for Nuclear Research

University Supervisors

Prof. A. Catrina Bryce, Dr. Martin W. Macauley

ABSTRACT

Operators of complex machinery must always think ahead to consider possible future operational threats to, or limitations of, the system. With this in mind, the ability to simulate and analyse the system in operation under potentially dangerous scenarios can be very useful, as it can make important predictions regarding its stability and safety. The following report details the work completed, by the author, while working with the Performance Evaluation Section of the Machine Protection and Electrical Integrity Group of the Technology Department (**TE-MPE-PE**) at the European Organization for Nuclear Research (**CERN**), from June 2011 to December 2011.

The main aim of the project was to design and construct a circuit model of a magnet powering system, specifically the Inner Triplet System (**ITS**) currently in use within the Large Hadron Collider (**LHC**), which had to be capable of accurately simulating the electrical and thermal transients following a quench within one of the system's superconducting magnet coils. The model was then to be used for the simulation and analysis of future, potentially dangerous, scenarios.

After the initial research and acquisition of relevant information, the design methods used involved: the modelling of the electrical circuit using Cadence® Allegro® Design Entry HDL (**DEHDL**) circuit design and modelling software; the simulation of the ITS system in operation using Cadence® Allegro® AMS simulator; the comparative analyses of simulated data with that of measured data using MathsWorks® MATLAB®; and the subsequent refining of the circuit model and the repetition of comparative analyses until accurate to within a specified accuracy tolerance.

The resultant comparative analyses of simulation data with recorded data proved that the constructed model could simulate the desired system scenarios to well within the required levels of accuracy. Subsequent analyses of a quench in the system, running at close to maximum allowable currents, predict that the system's magnet would 'self-protect' and the system would remain stable under these circumstances. However, in analysing scenarios in which a vital aspect of the system were to fail, catastrophic misdirection of current occurs and further analysis of these plausible events is called for.

With the successful completion of the specified aims, it can be concluded that DEHDL software can be used to adequately model the electrical and thermal transients following a quench in a high energy, complex powering system, containing superconducting magnets. It also follows that the circuit model is now available for future use when attempting to understand unexplained events occurring within the system or for the prediction of the system's stability and safety under particular scenarios.

TABLE OF CONTENTS

PREFACE

This report details the work completed for the University of Glasgow, Master of Engineering Course, 'Industrial Project EE5' (Glasgow) [1]. This course is a requirement, during the final year for completion of the Electronics and Electrical Engineering, Master of Engineering, degree course. The work was completed at the European Organization for Nuclear Research (**CERN**) during the period of June 2011 to December 2011.

The report will detail the progression of the project, particularly the development and proof of accuracy of the circuit model, the potential uses and importance of having such a model available, as well as analysis of hypothetical simulation results. The specific circuit that was modelled was the Inner Triplet System (**ITS**) within the Large Hadron Collider (**LHC**). Besides an overview of the project, the introduction will also include a brief history of CERN, the LHC and its intended design goals and purposes.

ACKNOWLEDGEMENTS

Having enjoyed both the work and the work environment, I feel it is necessary to begin with a short, but sincere, thankyou. Firstly, I would like to thank the University of Glasgow's Department of Electronics and Electrical Engineering, the head of this course, Prof. Charles N. Ironside, and both my University supervisors, Prof. A. Catrina Bryce and Dr. Martin W. Macauley, for allowing such a placement to be an integral part of the degree (Master of Engineering). Secondly, I would like to thank my employer, CERN, for giving me such a life changing opportunity. Special thanks go to Arjan Verweij, my contractor and supervisor, Emmanuele Ravaioli, my colleague and tutor, and Rüdiger Schmidt, Head of TE-MPE-PE*.

*Technology Department - Machine Protection and Electrical Integrity Group - Performance Evaluation Section

List of Figures

List of Tables

List of Acronyms and Abbreviations

General Engineering terms

ºC	Degrees Celsius
A	Amperes
B	Magnetic Field Strength
Cu	Copper
eV	Electron Volts
H	Henrys
I	Current
J	Joules
K	Kelvin
L	Inductance
L	Length
NbTi	Niobium-Titanium
Q	Charge
QP	Quench Propagation
R	Resistance
s	Seconds
t	Time
V	Volts
W	Watts
Ω	Ohms

Project Specific terms

ABM	Analogue Behavioural Modelling
ALICE	A Large Ion Collider Experiment
AMS	Analogue Modelling Simulator
ATLAS	Atlas Experiment
BCS	Bardeen Cooper Schrieffer theory
CERN	European Organization for Nuclear Research
CMS	Compact Muon Solenoid
EDMS	Engineering & Electrical Data Management Service
DEHDL	Design Entry High Definition Language
FWD	Free-Wheel Diode
FWT	Free-Wheel Thyristor
HTS	High Temperature Superconducting Current Leads
Istim	Current Stimulus
ITS	Inner Triplet System
FPA	Fast Power Abort
LEP	Large Electron Positron
LHC	Large Hadron Collider
LHC-CM	Circuit Modelling Group
LHCb	Large Hadron Collider beauty experiment
MQX*n*	Quadrupole Magnet
PC	Power Converter
PM	Post Mortem
PS	Proton Synchotron
Q*n*	Quadrupole Magnet
QPS	Quench Protection System
RRR	Residual Resistivity Ratio
RQ	Ripple Quadrupole
RQX	Ripple Quadrupole Power Converter
RTQX*n*	Ripple Quadrupole Power Converter
SPA	Slow Power Abort
SPS	Super Proton Synchotron
TE-MPE-PE	Technical Department - Machine Protection and Electrical Integrity Group - Performance Evaluation Section
Vstim	Voltage Stimulus

1 INTRODUCTION

1.1 Introduction

The project detailed in this report is the development, proof of accuracy and initial use of a circuit model of the Inner Triplet System (**ITS**) within the Large Hadron Collider (**LHC**) at the European Organization for Nuclear Research (**CERN**).

1.2 Background

This section briefly details the history of the organisation as well as giving a relevant introduction to the LHC, the ITS, and superconducting theory.

1.2.1 About CERN

The European Organization for Nuclear Research (CERN), located at the Franco-Swiss border north of Geneva, was founded in 1954 and was a collaboration of twelve European countries* [2]. Since its establishment, CERN has become one of the world's largest and most respected centres for scientific research, receiving regular international mainstream media coverage. As of today, CERN works with over 600 institutes and universities, from over 100 different countries worldwide. CERN employs nearly 3000 people and has approximately 10,000 visiting scientists including professors, lecturers, researchers and students [3].

As an organization, CERN has researched, discovered, invented and developed a variety of impressive and ground-breaking feats, including the creation of the world-wide-web in 1990. The organization's 'flag-ship' project, since the late 1950s has, however, been particle acceleration and collision. This began with the Proton Synchrotron (**PS**) in 1957, followed by the 6.9km long proton–antiproton collider Super Proton Synchrotron (**SPS**) in 1979, which gave way to the discovery of the $W^{\pm}$ and Z^{0} bosons in 1983. In 1989, the Large Electron Positron (**LEP**), a 27km collider was constructed, but made no significant discoveries. The LEP was shutdown in 2000, and was replaced by the Large Hadron Collider (**LHC**). The LHC is a proton-proton collider with two separate beams which cross at four unique collision points [2].

---

*Austria, Belgium, Bulgaria, the Czech Republic, Denmark, Finland, France, Germany, Greece, Hungary, Italy, the Netherlands, Norway, Poland, Portugal, the Slovak Republic, Spain, Switzerland and the United Kingdom.

1.2.2 The Large Hadron Collider

Constructed in the same tunnel as the LEP, the LHC (*Figure 1*) is approximately 27km in diameter, spanning the Franco-Swiss border, and is roughly 100m underground [4]. The LHC's designated purpose is to help physicists recreate the conditions present in the universe moments after its creation. This is done by colliding two particle beams, travelling close to the speed of light in opposite directions, thus releasing vast amounts of energy and breaking the particles into their most fundamental form. During these collisions, physicists study these fundamental particles and also try to discover/understand unknown/new particles - in particular the Higgs boson. Discovery of the Higgs particle is the main purpose of the LHC as it is crucial to confirm current theory on the fundamental laws of nature **i.e.** the Standard Model [4]. The Higgs boson is crucial as its existence will prove the theory of the Higgs field, which states that an invisible force (the Higgs field) exists and that any particle interacting with this field is given mass via the Higgs boson [5].

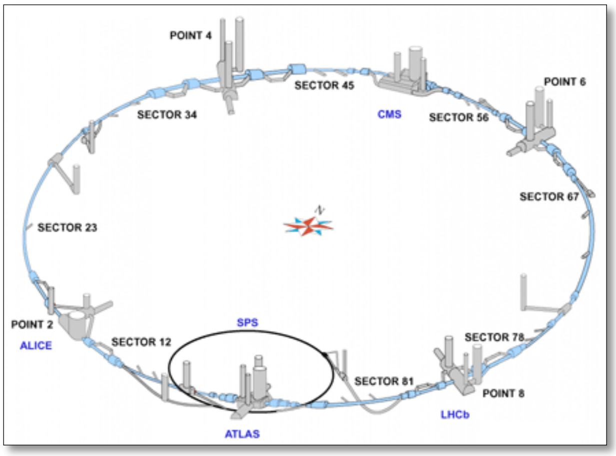

Figure 1: The Large Hadron Collider *[fig 1]*

The LHC accelerates particles close to the speed of light. This is in fact an impressive 99.9999991% of the speed of light, when operating at collision energy of 7TeV. These incredible energies/speeds are achievable due to magnetic fields produced by the superconducting accelerating electromagnets. These magnets are cooled to a temperature close to absolute zero, 1.9K. This allows the material of the magnet coils to reach a superconducting state which, due to not yet fully understood phenomena, gives the material zero electrical resistance [6]. The LHC ring is mostly constructed of superconducting magnets and contains 1232 dipole magnets (each up to 15m long) which bend the beam around the ring as well as 392 quadrupole magnets (each up to 5-7m long) which focus the beam before collisions. There are also 'squeeze' magnets to increase the chances of particle collision as well as non-superconducting correcting magnets throughout [6]. Of these magnets, the project covered in this report is related to the focusing quadrupoles, in particular the Inner Triplets, which are on either side of each collider.

1.2.3 Introduction to the Inner Triplet Systems

The Inner Triplet System (**ITS**) is the powering system for the superconducting quadrupole magnets, designed to provide the *final* focusing of the beams before collision. There is an ITS on either side of each of the four main collider experiments (ATLAS, CMS, ALICE and LHCb)*, ensuring the focusing of particle bunches in either of the opposing beams [7]. The system has two main circuit types: Type 1 is present in ATLAS and CMS experiments and Type 2, in ALICE and LHCb.

The ITSs are comprised of superconducting quadrupole magnets powered by surrounding circuitry. These magnets were designed and manufactured by two major research laboratories. They are given simple names Q1, Q2a, Q2b and Q3. Q1 and Q3 were developed by KEK** in Japan and Q2a and Q2b (identical) were developed by Fermilab*** in the United States of America [7]. The understanding and modelling of the characteristics of these magnets, both during normal superconducting operation and during a quench, has been a fundamental part of this project.

1.2.4 Superconducting Theory and the Quench of a Superconducting Magnet

A superconducting magnet is an electromagnet made from coils of superconducting wire. These coils, when cooled below a critical temperature, e.g. in the case of Niobium-Titanium (**NbTi**), 1.9K, achieve a superconducting state [8]. The cooling in the LHC is done via cryogenics, using a liquid helium bath [6]. When a material is in a superconducting state, consistent conditions occur, which allow current to flow with zero electrical resistance. This phenomenon, with current understandings known as BCS (Bardeen Cooper Schrieffer) theory [9], allows for large currents to be generated with relatively low applied voltages due to pairs of electrons 'Cooper pairs' never interacting or scattering within the superconducting materials lattice [9]. These large currents allow for strong magnetic fields to be produced by the magnets, used to accelerate particles with great amounts of energy. A superconducting magnet is, however, susceptible to a debilitating phenomenon known as a 'quench'. A quench occurs when a magnet crosses a threshold of a critical field, critical current, critical temperature or critical strain [10]. During a quench, a part of the magnet heats up and makes a transition from superconducting state back to its normal resistive state. This creates a 'hot-spot' which subsequently heats up the surrounding area of the

---

*ATLAS - Atlas Collider Experiment, CMS - Compact Muon Solenoid, ALICE - A Large Ion Collider Experiment, LHCb - Large Hadron Collider beauty. **KEK - *Korporata Energjetike e Kosovë, Japan* ****Fermilab - U.S Department of Energy's Fermilab, United States of America.*

magnet forcing the material to return to its normal state (solid lattice with inherently electrically resistive properties). The resulting avalanche effect and the quench's overall 'movement', is known as 'quench propagation'. A magnet quench and its propagation are both relatively unknown phenomena and, due to the possible damage to the magnets (previously known to have halted operation of the LHC for a year in September 2008), are at the forefront of engineering research at CERN [11].

1.3 Aims and Justification of the Project

The prime purpose of this project was to fulfil curriculum requirements of the Master of Engineering degree course at the University of Glasgow [1]. On applying to CERN for a 6 month internship, this project was offered to me. I, the author, considered this project worthwhile as it involved working for a world renowned scientific organization as well as the fact that the project itself would allow further development of skills attained at university and the opportunity to work with experts in the field. More specifically, the project would make a contribution to CERN's understanding of the stability of the LHC's powering systems as well as the, still largely unknown, phenomenon of the quench of a superconducting magnet.

1.3.1 Project Aims

- Design, develop and construct a working circuit model of the LHC's ITS, capable of accurately simulating the electrical and thermal transients, following the quench of a superconducting magnet within the system.
- Following the successful completion of the model, use it to analyse the stability of the ITS, during a quench in the system, with the presence/occurrence of system defects/failures or during theoretical worst case scenarios.

1.4 Summary of Relevant Previous Work

The Circuit Modelling Group **(LHC-CM)** is a collaboration of several sections within the Machine Protection and Electrical Integrity Group **(MPE)** and its goal, amongst others, is to design and develop an accurate model of each type of superconducting magnet, for quench analysis, as well as each type of powering system circuits for operation, stability and safety analysis.

Prior to this project, several simpler powering systems models (e.g. RQ4 and RQ10) had been modelled in a similar manner [12]. However, it was thought by their designer, Emmanuele Ravaioli, that the accuracy of the quench modelling could be improved.

1.5 Methodology

The methods used throughout the design and final analysis included the initial research and acquisition of the ITS and its corresponding parameter data; the design and development of a circuit model, using circuit schematic drawing software to generate usable PSpice® netlist code; the simulation of the circuit model in operation using PSpice® simulation software; the comparison of simulation results with measured LHC data; and the subsequent debugging and advancement of the circuit model until comparative studies proved accurate. This process was repeated for both the development of a basic circuit model and the further development and inclusion of circuit complexities.

Following the completion of the circuit model, simulation software was used to analyse the circuit's operation during a range of plausible scenarios.

1.6 Project Limitations

It is important to mention that the choice of circuit to model, the software used, methodology, figures of merit and analytical processes were all defined by the employer and little to no deviation was allowed to ensure consistency with previous circuit modelling projects.

1.7 Overview of the following Body of Work

The following body of work will begin by detailing, in depth, the Inner Triplet System, its components and its general operation. This will lead on to the initial development of a basic circuit model and the subsequent simulation results. Following this, the development of the complex electro-thermal model will be covered as well as its accuracy in the modelling of a quench in the system. Finally, a full analysis of simulations run, testing the system during a quench as well as plausible, potentially dangerous, scenarios, will be included.

2 Understanding the Inner Triplet System

2.1 The Inner Triplet System

The Inner Triplet System (**ITS**), specifically the magnet powering circuit, is referred to as the ripple-quadrupole (**RQX**) circuit. It is the system responsible for generating the energy required to produce stable and strong magnetic fields within the focusing quadrupoles Q1, Q2a, Q2b & Q3. The magnets are powered by three power converters in a unique nested loop circuit design. This nested loop design allows for lower powered sources to produce the high currents required. There are a number of diodes for safe dissipation of energy, but there is no dedicated energy extraction loop. A simplified schematic is shown below (*Figure 2*).

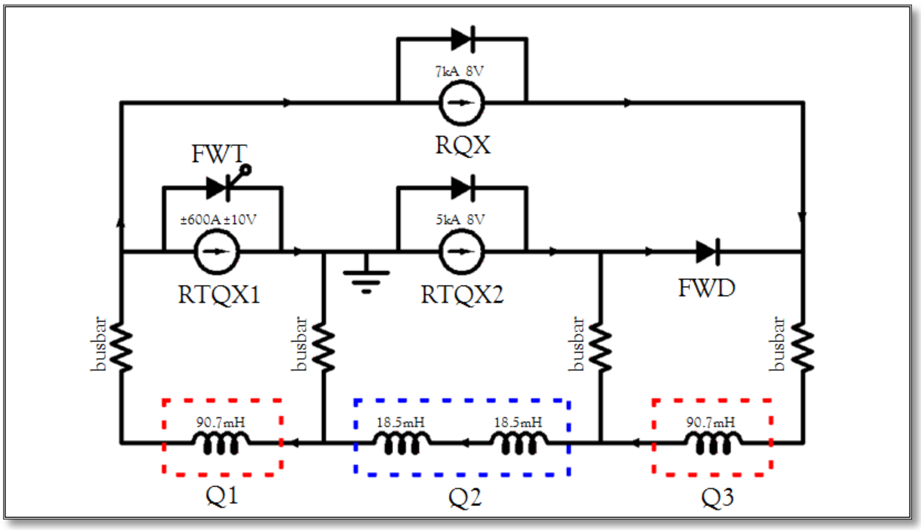

Figure 2: Simplified Schematic of Inner Triplet System (Type 1)

As previously mentioned (**Section 1.2.3**), the ITSs are on either side of each of the four main collider experiments. There are, however, two forms of the system. **Type 1**, used on both sides of the ATLAS and CMS collider experiments, is as above (*Figure* 2) with the RTQX1 PC and FWT in parallel with the Q1 magnet. Whereas, **Type 2** (*Figure* 3), used on either side of the ALICE and LHCb collider experiments, has the RTQX1 PC and FWT in parallel with the Q3 magnet. There are also four of each type of ITS present in the LHC and to prevent confusion a common referencing system is used throughout the report when referring to a specific circuit. This is based on the eight sector points on the LHC (*Figure* 1) which are named 1-8 counting clockwise around the accelerator from ATLAS. For example, 'RQX.L1' would refer to the ITS on the left side of the ATLAS collider experiment and 'RQX.R5' would refer to the ITS on the right side of the CMS collider experiment.

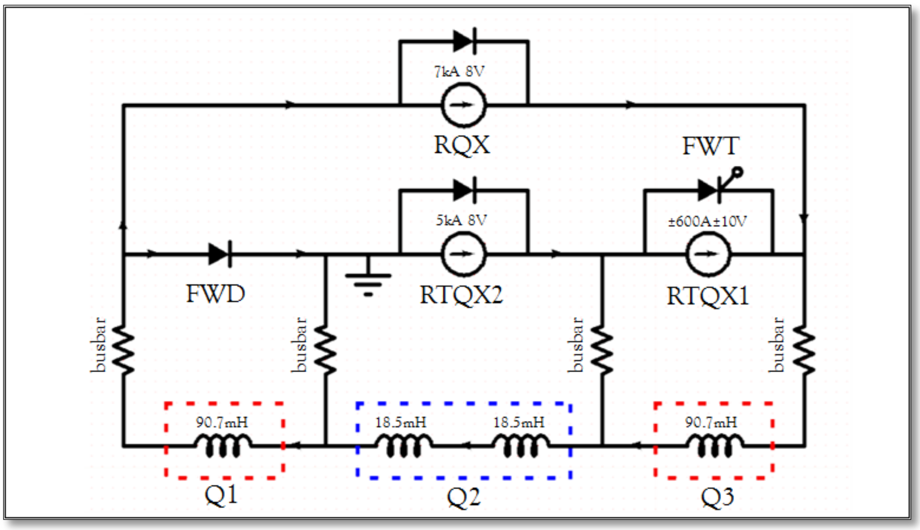

Figure 3: Simplified Schematic of Inner Triplet System (Type 2)

2.2 Circuit Components

As shown in *Figure 2* and *Figure 3*, The RQX circuit contains several high energy components. These include: superconducting magnets; high current power converters with corresponding diode paths; free-wheel thyristors; free-wheel diodes and current leads/busbars. This section will list and briefly describe their characteristics.

Superconducting Electromagnets

MQXA – The MQXA magnet, developed by KEK*, has an inductance of 90.7mH and a maximum operating current of 6.8kA [13]. This type of magnet also has full length quench heaters.

MQXB – The MQXB magnet, developed by Fermilab**, has an inductance of 18.5mH and a maximum operating current of 11.9kA [14]. This type of magnet also has full length quench heaters.

Power Converters

RQX (7kA 8V) – The RQX power converter is a high energy converter which produces 7kA at a low 8V. Its corresponding diode path is two block circuits of 20x 245NQ015R [ds1] Schottky diodes, made by International Rectifier, in parallel [15].

RTQX2 (5kA 8V) – The RTQX2 power converter is a high energy converter which produces 5kA at a low 8V. Its corresponding diode path is one block circuit of 20x 245NQ015R [ds1] Schottky diodes, made by International Rectifier, in parallel [15].

---

*KEK - *Korporata Energjetike e Kosovë, Japan*
***Fermilab - U.S Department of Energy's Fermilab, United States of America.*

RTQX1 (±600A ±10V) – The RTQX1 power converter is a bi-polar, low energy converter which produces 600A at a low 10V. Its corresponding thyristor path consists of two TZ425N [ds2] phase controlled thyristor modules, made by EUPEC, in anti-parallel [15].

Free Wheel Thyristors

FWT – The FWT current loop consists of two T3709N04 [ds3] phase controlled thyristor modules, made by EUPEC, in anti-parallel [15].

Free Wheel Diodes

FWD – The FWD current loop consists of two D4457N [ds4] power rectifier diodes, made by EUPEC, in parallel [15].

Current Leads/Busbars

HTS Leads – The HTS leads, designed by CERN, are current leads handling up to 13kA which connect normal state wires, 'at warm', to superconducting wires, 'at cold' [15].

2.3 Circuit Current Flow during Normal Operation

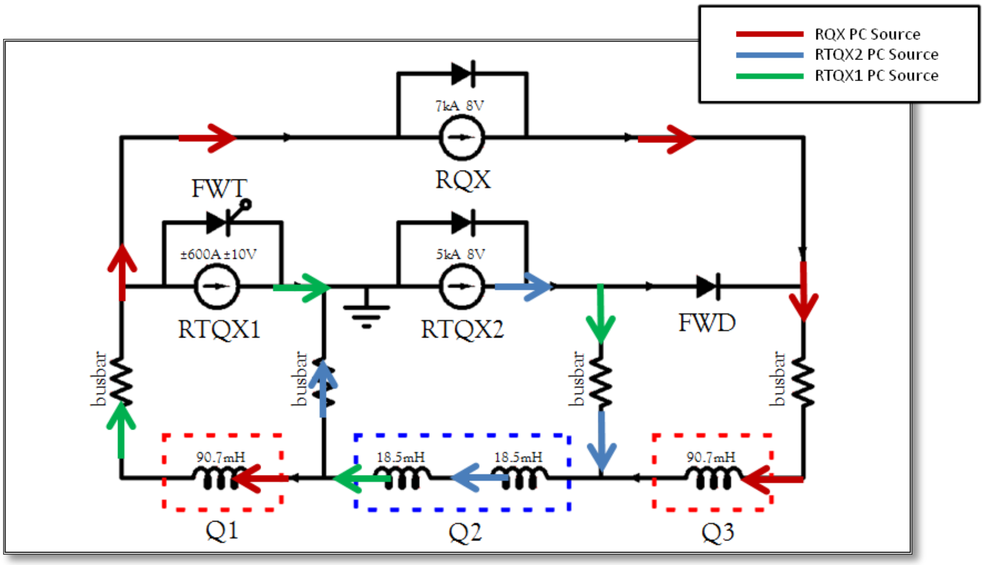

Figure 4: Flow of Current during Normal Operation, RTQX1 positive

The RQX circuit provides the electromagnets with the current levels required to produce the magnetic field. It does this in a nested loop operation with the RQX power converter (**PC**) powering the MQXA magnets, Q1 & Q3, and both RQX and RTQX2 PCs powering the MQXB magnets, Q2a and Q2b. The RTQX1 PC shown (*Figure* 4) , is a bi-polar balancing source, which produces either, a positive current, to increase the current flowing through the Q1 magnet, relative to Q3, or a negative current (*Figure* 5) to increase the current flowing through the Q3 magnet, relative to Q1.

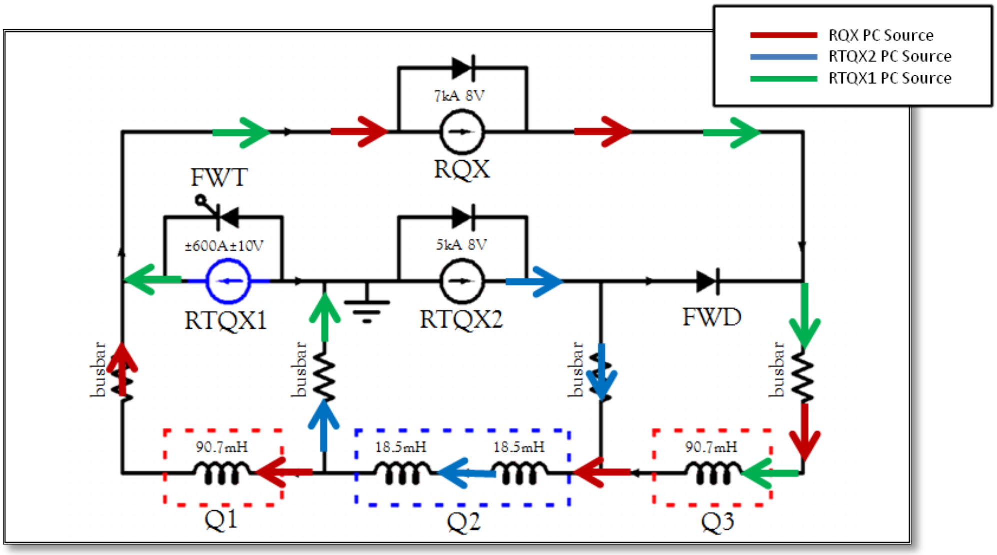

Figure 5: Flow of Current during Normal Operation, RTQX1 negative

2.4 Current Flow in the Circuit during a Quench

When a magnet in the system is subject to a quench, the operation of the system alters. On detection of a quench, the quench protection system **(QPS)** sends a signal to initiate a fast power abort **(FPA)** of all PCs, and the firing of all quench heaters. Quench heaters are designed to force a quench upon the whole magnet uniformly, in terms of propagation, to prevent any potential damage. This is done by heating the entire length of the magnet coils to above superconducting temperatures [16]. The QPS also triggers the FWT, forcing the current, now produced by the stored energy in the magnets, to flow through all free-wheel paths in order to dissipate the energy as quickly and as safely as possible. This new current flow during this stage of a quench, with RTQX1 set positive, is shown below (*Figure 6*).

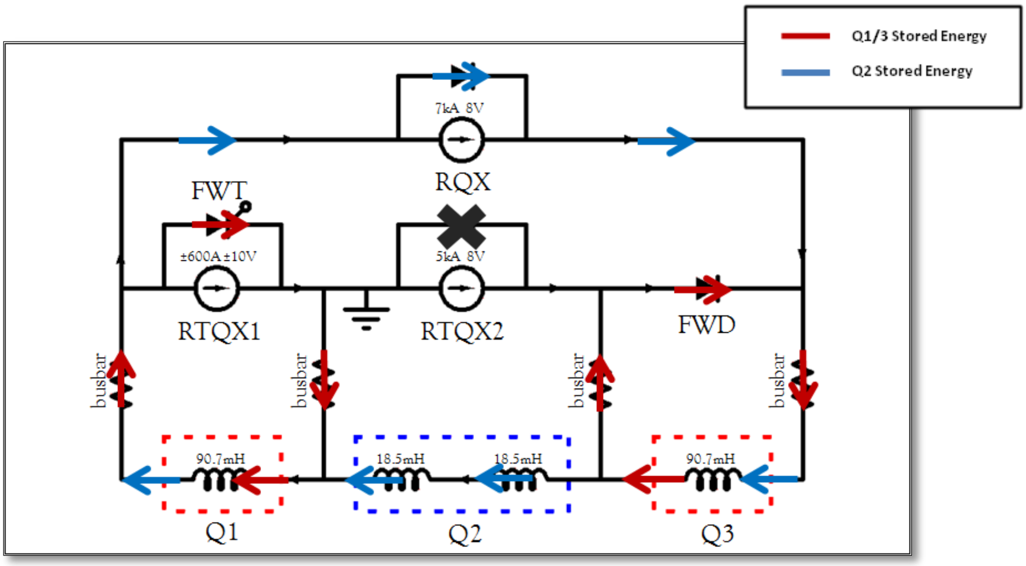

Figure 6: Flow of Current during a Quench, RTQX1 positive

3 Circuit Modelling/Simulation Software

3.1 Cadence® Allegro® Design Entry HDL

The circuit drawing/netlist generating software used was that of Cadence® Allegro® Design Entry HDL **(DEHDL)**. This is very robust software, similar to that of Cadence® OrCad®, in which a circuit schematic can easily be constructed by means of placing symbols, 'parts', in the main schematic window, which represent models of genuine components, with specific parameters, and simply connecting them via wiring. This can be used to draw any variant of electrical circuit, as long as the parts are available or programmable.

3.2 Cadence® Allegro® AMS simulator

To simulate the operation of a drawn circuit, AMS Simulator **(AMS)** was used in conjunction with DEHDL. AMS simulator uses PSpice® technology [17] at the core, which provides fast and accurate simulations. It provides a great variety of simulation options such as parametric sweep/Monte Carlo analysis and allows for plotting resultant data in any desired graph format. This provides exceptional means for data analysis and circuit debugging.

3.3 MathWorks® MATLAB®

For ease of plotting extracted data files and for comparing simulation data with recorded LHC events, MathWorks® MATLAB® was used. MATLAB® is powerful mathematics software capable of computing calculations with large data files. This capability was necessary due to some simulations producing in excess of 300,000 data points.

3.4 General Use Software

Throughout the project, several other major software packages were used, including Microsoft® Office. In particular Microsoft® Excel was used for equations/calculations and general spread sheet work.

CERN also uses a variety of databases for file storage and project documentation. These were used to access a wide variety of information, from original mechanical drawings and component parameters to that of recent LHC events. Database examples include: Post Mortem Browser, TIMBER, EDMS and the LHC Electrical Circuits Database.

4 DEVELOPMENT OF THE SIMPLIFIED RQX CIRCUIT MODEL

4.1 Design of Simplified RQX Circuit Model

The initial proposed design of the simplified RQX circuit model was that of a circuit based on the simplified schematic, previously shown in *Figure 2*. The design was then improved upon so that the model would include: the separate diodes for each 'block'; the resistances of the non-superconducting cables; a triggering circuit for the thyristors; and parasitic resistances and capacitances.

4.2 Acquisition of Circuit Component Parameter Data

Before construction of the design model, it was important that the required relevant data was found. This proved troublesome and time consuming, due to the incompletion of CERN's databases, but was eventually managed. Date sources included: CERN Circuit Model Layout Database; CERN EDMS Database; documents produced by the systems commissioners; and component manufacturer's datasheets.

4.3 Construction of Simplified RQX Circuit Model in DEHDL

This section details the methods used for the modelling of each component in the circuit and the resultant schematic, based on the designed model of the constructed model.

4.3.1 Modelling of the Superconducting Magnets

During normal operation of the ITS, its magnets (electromagnets) are already cooled to a superconducting state and thus have zero electrical resistance. This allows for the simple modelling of the magnet with that of a default part model for an inductor, representing the inductive properties of the wound electromagnetic coils.

4.3.2 Modelling of the Power Converters

The PCs in the system are not current sources, however, for ease of modelling, the choice of using representative ideal current sources, with programmable outputs, was made. This allowed for the accurate reproduction of the system's powering during an array of plausible scenarios.

4.3.2.1 Programming PC Current Level Stimuli

During the commissioning and testing of each magnet circuit in the LHC, a defined series of tests must be run to confirm the circuit is fully operational without faults. Specific to the RQX circuit, there are a variety of tests, ranging from a minimum safe operation current to a maximum safe operation current, as well as the testing of PC power aborts, both fast and slow, and the firing of magnet quench heaters. A basic graph (*Figure 7)* details some of the most common commission tests. The full list of tests, with exact corresponding current 'ramping' rates and plateau levels/lengths, can be found on EDMS – Inner Triplet System [18].

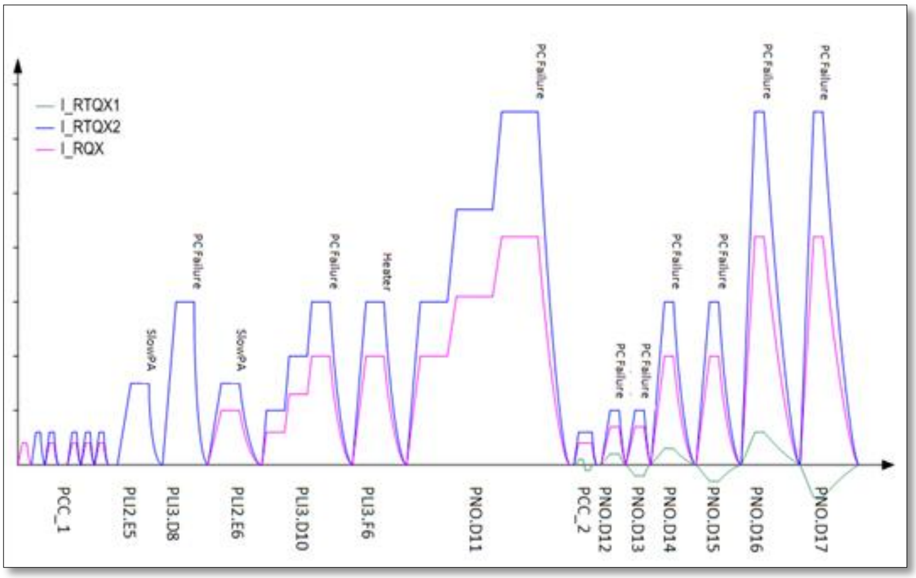

***Figure 7: Plot of Different Commissioning Tests for Quadrupole Magnets** [fig 2]*

In simulating these currents, due to the non-linearity of the current, a given stimulus had to be manually programmed for each PC. This was possible due to stimuli operated source models available in DEHDL, such as 'Vstim' or, in the specific case of the modelled PCs, 'Istim'. However, for ease of manipulating the current, it was found that manually editing the stimulus text file produced desirable results. *Figure 8* is an example of a programmed stimulus, and corresponding current plot. This is specific to the RTQX2 PC, running test PNO.D16. Stimulus code, similar to that shown in *Figure 8*, was programmed for each PC for every major test and can be found in **Appendix F.1**.

```
.STIMULUS RTQX2_PNO.D16 PWL
+TIME_SCALE_FACTOR = 1
+VALUE_SCALE_FACTOR = 1
+ ( 0, 0 )
+ ( 31, 0 )
+ ( 80, 200 )
+ ( 120, 200 )
+ ( 937.5, 3510 )
+ ( 960, 3510 )
+ ( 960.05, 0 )
+ ( 10k, 0 )
```

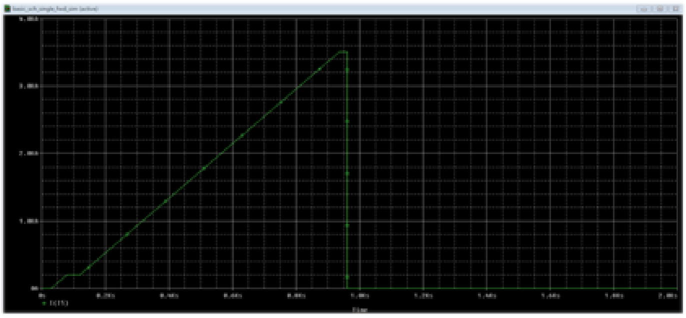

Figure 8: Istim Current Source Stimulus Code Example for Test PNO.D16

4.3.3 Modelling of the Diodes

The diodes were initially implemented using a model part available in default libraries of DEHDL. However, for the accurate modelling of the diodes in use within the ITS, AMS Model Editor was used. This allowed for a diode, being a pre-programmed part option, to be accurately modelled via the in-built iterative optimisation software. To carry this out, known parameters and graphs, as defined in the manufacturer's datasheets, were entered into the Model Editor and the optimisation option was run. An example (*Figure 9*) of this process is shown below. It is clear that, for a few defined points in a variety of device operations, the model editor generates, through optimisation, a diode model with characteristics that follow the user defined points as closely as possible. The software then generates all of the parameter values specific to the internal design of the pre-programmed diode model.

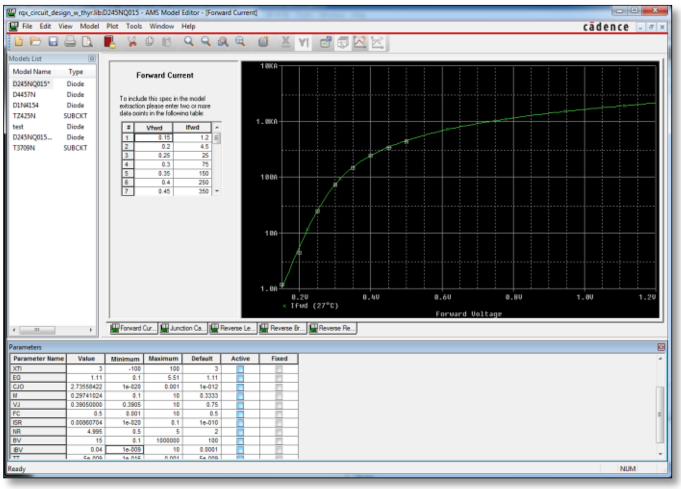

Figure 9: Screenshot of AMS Model Editor Iterative Parameter Optimisation

After implementing the component characteristics as defined by the manufacturer, the resultant parameters for both types of diodes were produced. *Table 1* shows an excerpt of a table of the generated parameters corresponding to a D234NQ015R Schottky diode [ds1]. The parameters for both diode types can be seen, in full, in **Appendix C.1.1** and **Appendix C.1.2**.

Table 1: Excerpt of Model Editor Parameters for D245NQ015R Schottky Diode

Parameters	Abb	Values	
Saturation Current	IS	1.93186E-02	A
Emission Coefficient	N	1.15684E+00	
Resistance	RS	2.37362E-04	Ω
High-Inject Knee Current	IKF	2.60259E+02	A
Saturation Current Temp coeff	XTI	3.00000E+00	

4.3.4 Modelling of the Thyristors

Due to AMS Model Editor not having an available pre-programmed model of a thyristor, the iterative optimisation procedure could not be used. However, in looking up the parameters used in modelling the average thyristor, it was found that every parameter was defined in the manufacturer's datasheet. This proved easier than modelling the diodes, but less accurate. A simple picture of how the parameters were manually entered into the AMS Model Editor is shown below (*Figure 10*). The corresponding parameters for both, TZ425N [ds2] and T3709N [ds3] thyristors can be found in **Appendix C.1.3** and **Appendix C.1.4**, respectively.

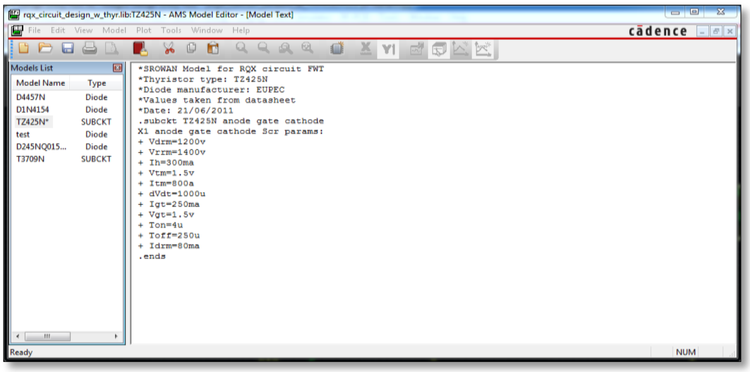

Figure 10: Screenshot of Manual Parameter Input in AMS Simulator

4.3.4.1 Thyristor Triggering

A thyristor is a bi-stable switch, acting similar to an open-circuit when no current is applied to the gate, and acting as a diode, in forward bias, when sufficient current is applied. The thyristor part models, within DEHDL, follow the same principle and require additional circuitry to be constructed to trigger/turn on the thyristors.

Two triggering methods were devised. The first (see **Appendix E.2**) was constructed of a current source in series with a resistor, applying current between the gate and the anode; the second (see **Appendix E.3**), made use of a simple voltage source applying the threshold voltage across the gate and cathode. The latter construct, though not designed until after the implementation of the electro-thermal model (see **Chapter 6**), was eventually chosen as it proved to be the more efficient in terms of bleeding unwanted current into the circuit and in simulation convergence rates.

4.3.5 Modelling of the Circuit Impedances

As all of the circuit impedances in the designed simple circuit model were of constant values, the modelling throughout merely involved the inclusion of the DEHDL's default model for parts where necessary. The following subsections specify all the included impedances and how their values were either calculated or found.

4.3.5.1 Busbar Resistances

After the successful implementation of the diode and thyristor models, the circuit was further advanced by including accurate values for the busbar resistances. These values, though proving hard to find at first, were eventually acquired from the LHC Electrical Circuits Database which listed recent resistance measurements across each PC. Due to the nature of the circuit, finding the busbar resistances from the database was simply a matter of halving the recorded values. As the busbar values in each LHC sector's RQX circuit vary greatly, those used in a specific simulation will be detailed when necessary. An exceprt of the full list of busbar resistances, specific to that of the RQX.L8 circuit can is shown in *Table 2*. The full list of busbar resistances can be found on CERN's Electrical Circuit Layout Database.

Table 2: Excerpt of Variable Parameter List as used in Circuit Model for RQX.L8

Parameters	Abb (as used)	Values (Ω)
RTQX1 Copper Bar lead resistance	RCOPPERBAR	160u
Q1 Busbar resistance	RRQXBUSQ1	550u
Q2a Busbar resistance	RRTQX2BUSQ2A	685u
Q2b Busbar resistance	RRTQX2BUSQB	685u
Q3 Busbar resistance	RRQXBUSQ3	550u

4.3.5.2 Cable Resistances/ Parasitic Capacitances

To reduce inaccuracies, further complexity was introduced, including non-busbar cable resistances as well as parasitic resistances and capacitances. Regarding the parasitic components, their existence and positions were theorised and given commonly accepted values. For the cable resistances, taking into account the resistivity and dimensions of the cables, calculations were done using Microsoft® Excel. To acquire the results (see **Appendix C.2**) the following resistance equation (*Equation 1*) was used. The resistivity used was an industry accepted value for a temperature of 293K and the cable dimensions were found using the EDMS database.

$$\textit{Equation 1:}\quad \boldsymbol{R_{cable} = \rho_{cable}\left(\frac{L_{coil}}{A_{coil}}\right)}$$

4.4 Circuit Parameter List

DEHDL has a parameter function, allowing for components to be given named variable values which can be easily assigned to several components allowing quick alteration of variable parameters. This option was used extensively, listing parameter variables wherever possible.

4.5 Schematic as constructed in DEDHL

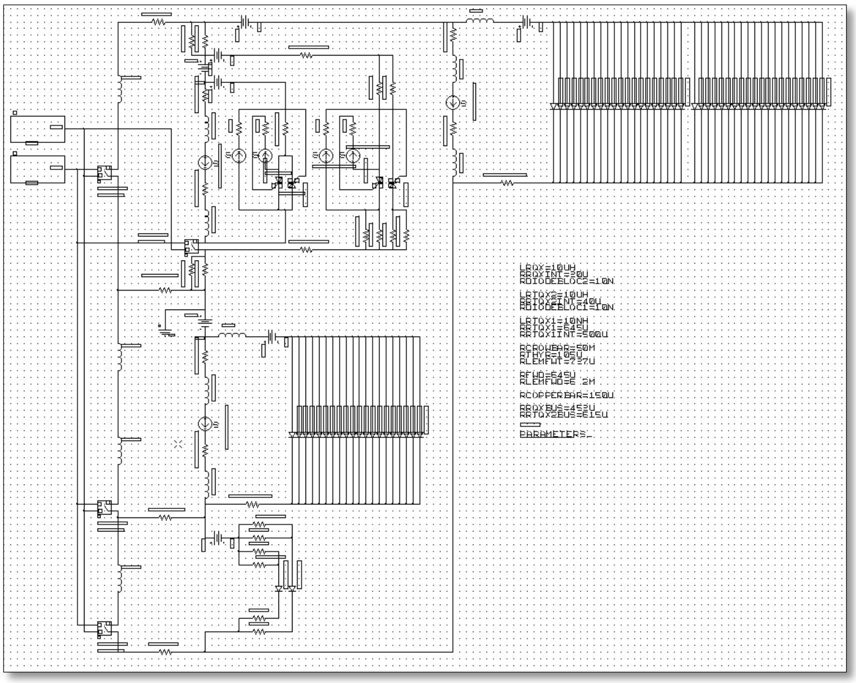

Figure 11: Simplified Schematic Constructed in DEHDL

Figure 11 shows the final revision of the simplified circuit model as constructed in DEHDL. This proved successful in compiling and generating netlist code for simulation without any major problems.

4.6 Problems Encountered

In the initial stages of development, using the schematic design software DEHDL proved to be troublesome, as it is not very 'user friendly', has tedious controls and is not, in any way, intuitive. Another major problem was having to resort to, in some cases, 'trial and error' parameter sweeps for debugging, as this was very time consuming and not always fruitful. Apart from these, the overall progression in development of the simplified circuit model was fairly consistent with that predicted.

However, the acquisition of data, component parameters and characteristics, was the main cause for delay e.g. finding no information on any database then having to contact and arrange meetings with original designers/those responsible. This was, for the most part, due to the scale of the projects run at CERN, as there are a great number of circuit information/component databases, but not all sections have been completed.

5 SIMPLIFIED MODEL SIMULATION RESULTS

5.1 Initial Simulation Results

The following section briefly details the results of initial model simulations when compared to LHC recorded data. The following plots show initial results of simplified model simulations, specifically those with circuit variable parameters of RQX.R5.

5.1.1 RQX.R5, PLI3.D10 Test - FPA@50% Current, Main 2 PCs Active, RTQX1 Off

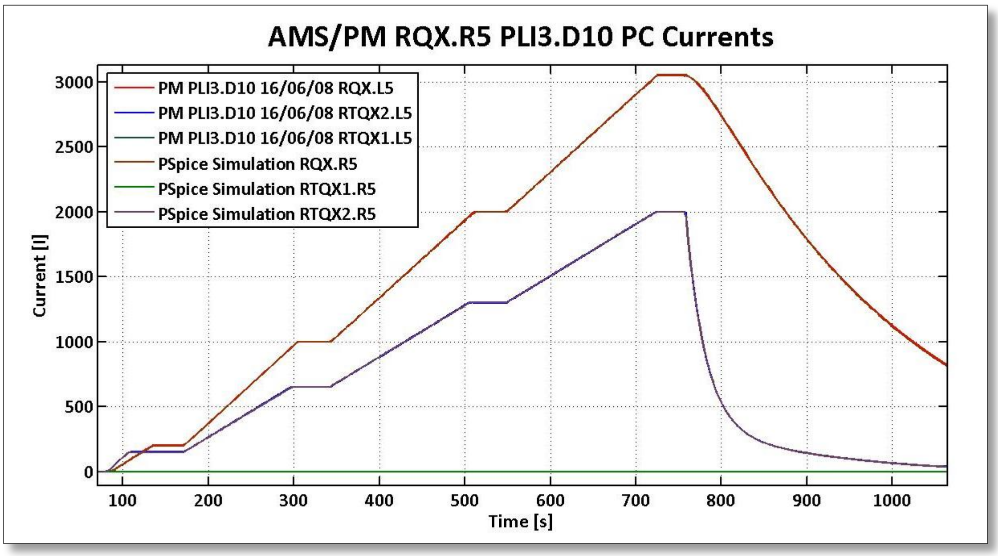

Figure 12: RQX.R5 PLI3.D10 Simulation using Simple Circuit Model

The comparison of a simulation, programmed to commissioning test PLI3.D10, with recorded LHC Post Mortem **(PM)** data *(Figure 12)*, showed the ability to program near exact ramping up/plateau conditions during the initial stages of the test, allowing for accurate analysis of magnet charging times. It was also apparent that, at the point a 'fast power abort' **(FPA)** is triggered, the simulation followed the discharge characteristics of recorded data to an impressive accuracy. As the discharge curve is heavily weighted on the L/R time constant, the simulation showed that the path resistances had been modelled correctly, as the magnets' inductances were taken as a constant throughout.

5.1.2 RQX.R5, PNO.D12 Test - FPA@10% Current, All 3 PCs Active, RTQX1 Positive

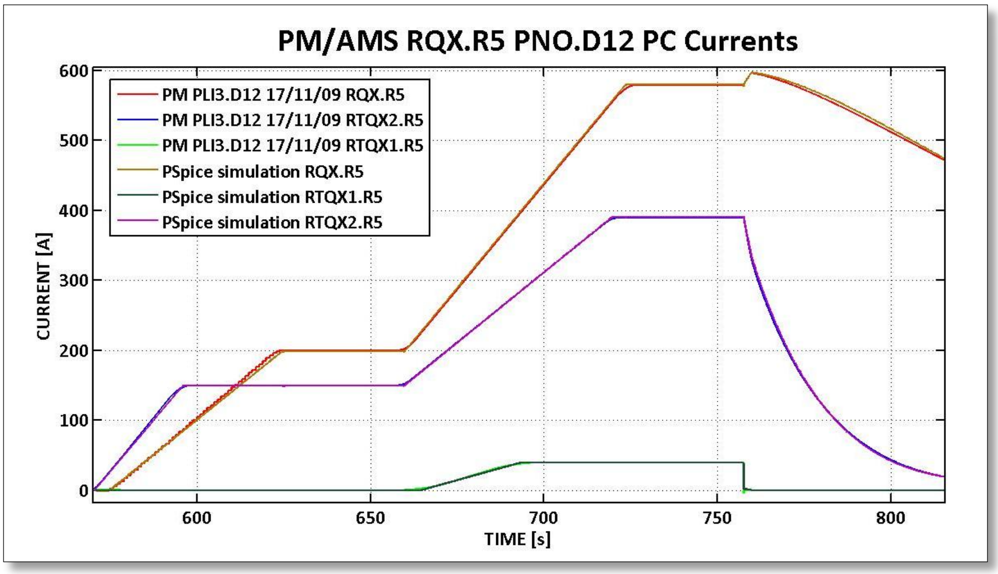

Figure 13: RQX.R5 PNO.D12 Simulation using Simple Circuit Model

The comparison of a simulation, programmed to commissioning test PLI3.D12, with LHC PM data *(Figure 13)*, again showed impressive agreement throughout, with the exception of a minor discrepancy in the transfer of current from the RTQX1 current loop to the RQX current loop, just after the point of triggering an FPA. Further 'tweaking' of variable parameters could have been carried out to manually improve accuracy but, due to this error being within the standard deviation of all ITS circuits, further progression in model complexities was deemed more of a priority.

5.2 Summation of Initial Comparative Results

The initial comparative results were found to be acceptable for this stage in the model development and progression was deemed more important than the constant reiteration of variable parameters which gave minimal increase in accuracy.

6 Development of the Electro-Thermal Model

6.1 Design of the Electro-Thermal Model

The proposed design for the electro-thermal model was as shown (*Figure 14*).

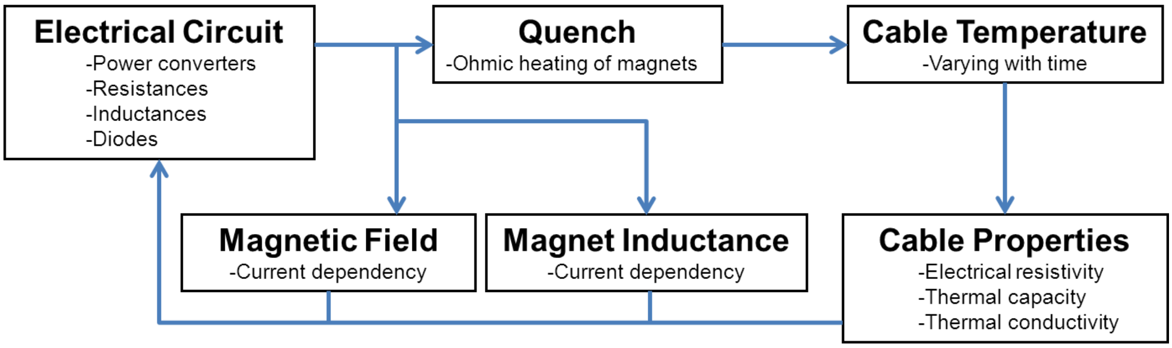

Figure 14: Block diagram of the design of the Electro-Thermal Model

As shown in *Figure 14*, the intended electro-thermal model took into account a variety of factors, not previously included. These factors included the current dependency for magnetic field and magnet inductance, as well as the variance of the magnetic coil temperature, which in turn affected the values for electrical resistivity, thermal capacity and thermal conductivity. To model a quench correctly, it was important that the electro-thermal model was accurate and designed specifically to the magnet's characteristics.

6.2 Acquisition of Magnet Properties and Heavily Weighted Parameters

The accuracy of the calculations done by the ABM components was heavily dependent on the parameters used. These included accurate magnet properties/dimensions as well as the delay of QPS triggering and quench propagation velocity. This section will detail the properties and values found.

6.2.1 MQXA Magnet Properties

Arguably, the most important and heavily weighted parameters are those of the mechanical properties and dimensions of the magnets. These values were taken from the initial commissioning/testing reports of the magnets as well as original mechanical drawings and design parameters.

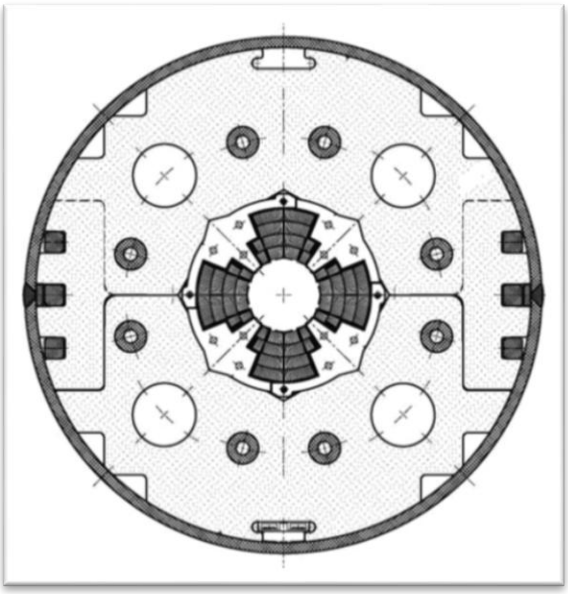

Figure 15: Cross section of the MQXA Quadrupole Magnet [fig 3]

Above (*Figure 15)* is the cross section of the MQXA magnets showing the amount of coil windings as well as the dimensions of the magnet and the magnet's construction and 'yoke' (casing). Using the derived values of magnetic transfer function and ratio of Cu/NbTi, along with other information, found on CERN's wide range of databases, regarding the magnet's mechanical properties, the following table (*Table 3)* was constructed, listing all important parameters for the MQXA magnets.

Table 3: Parameters of the MQXA Quadrupole Magnet

MQXA Parameters			
Coil	Inner	Outer	
Total wire length	~1550	~1650	m
Diameter of strand	815	735	um
No. Strands	28	33	
Insulation Thickness	50	/	um
Inductance	90.7	/	mH
Transfer function	1.203	/	
Ratio Cu/NbTi	1.2	1.9	
RRR	193	226	

6.2.2 MQXB Magnet Properties

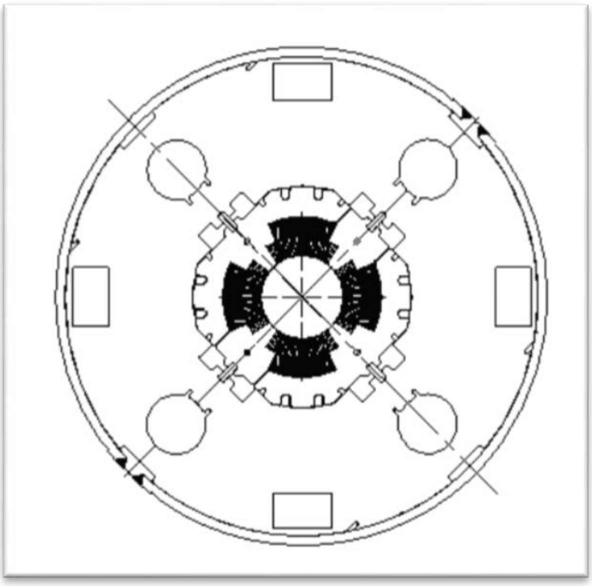

Figure 16: Cross Section of the MQXA Quadrupole Magnet [fig 4]

In a similar manner to the MQXA magnets, the properties for the MQXB magnets (*Figure 16)* were found and are listed in *Table 4*.

Table 4: Parameters of the MQXB Quadrupole Magnet

MQXB Parameters			
Coil	Inner	Outer	
Total wire length	672	760	m
Diameter of strand	808	650	um
No. Strands	14	16	
Insulation Thickness	25	/	um
Inductance	90.7	/	mH
Transfer function	1.203	/	
Ratio Cu/NbTi	1.3	1.8	
RRR	85	85	

6.3 Principles of Quench Modelling

During a quench, the superconducting coils within the magnet return to a normal resistive state in which they have a non-zero electrical resistance. This is caused by the formation of the 'hotspot' (detailed in **Subsection 1.2.4)**. To accurately model a quench, a thermal model was to be implemented to account for the sudden temperature change and the inherent rise in corresponding electrical resistance.

Due to the linear nature of basic temperature equations, it was found that, by manipulating Analogue Behavioural Model (**ABM**) components within DEHDL, an equivalent electro-thermal model could be constructed.

6.3.1 Quench Protection System

The aforementioned QPS system is designed to detect a quench or hot spot as soon as possible and then trigger the 'firing' of the magnets' quench heaters. This, however, is subject to an electrical timing delay which had to be taken into account in the circuit model. The delay is dependent on the magnet in question and from interpreting graphs of measured LHC data the value for each magnet in the ITS was found to be as follows (*Table 5*):

Table 5: List of delay in quench heaters for each magnet type

Magnet Type	Delay Time (ms)
Delay in MQXA	800
Delay in MQXB	400

6.3.2 Taking into Account Quench Propagation Velocity

Quench Propagation (**QP**) is a phenomenon not yet understood by science. Its direction and velocity is affected by almost all parameters of a magnet e.g. dimension, inductance, magnetic field, current, temperature and strain. It is also apparent that it follows no known function and thus cannot be accurately modelled. However, basic estimations for the purpose of quench modelling can be implemented in the calculation of electrical resistance within a coil. The function was subsequently advanced by testing an array of theorised options.

Linear relationship

Initially, the function, taking into account the QP, was estimated as a linear relationship. This produced a linear increase in electrical resistance with time across the duration of a quench event. Though sufficient for circuit model testing, this was far too inaccurate for quench analysis.

Exponential relationship

Assuming a quench initially propagated with a slow velocity, which was subject to a further exponential increase in velocity due to an 'avalanche' effect in hot-spots, an exponential Quench Factor was thought to be possible. Simulations, however, proved less accurate than a linear estimation.

Negative inverse exponential relationship

With the quench heaters fired, quenching the whole magnet as uniformly as possible, it was theorised that in the initial stages of the quench, due to more space being available within the magnet for QP to occur, the velocity was exceptionally high. Further thoughts lead to the belief that the QP velocity would, after a certain time, reach a saturation point as the available space for QP began to run out. To model this theory, implementing a devised negative inverse exponential function took place. The result, though somewhat opposite to the previous theory, proved very successful.

Following this success, the addition of variables to allow for other magnet forms was included, giving a 'fit function' suitable for near accurate estimation of QP velocity with time, assuming the use of quench heaters.

6.3.2.1 Quench Factor Function

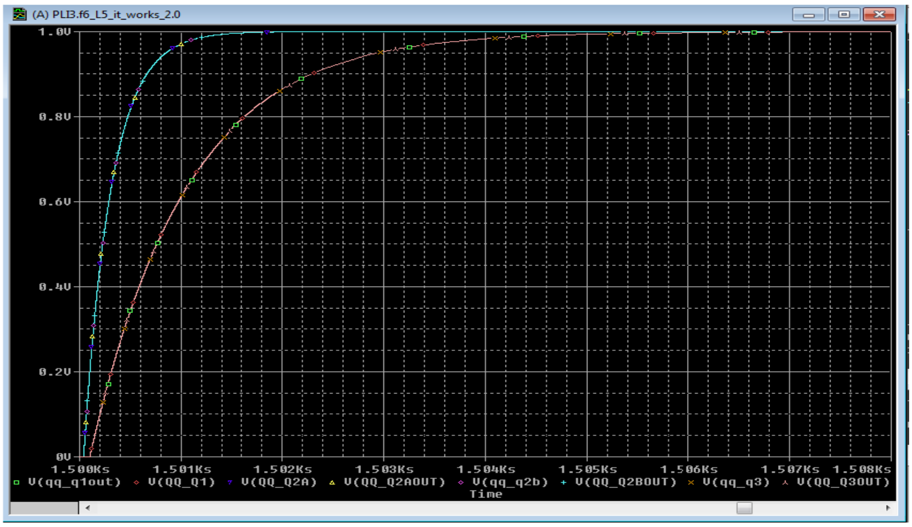

Figure 17: Plot, as seen in AMS simulator, of the Quench Factor function during a quench simulation.

Figure 17 shows the function (*Equation 2*) developed to determine the percentage of the magnet that was quenched with respect to time.

$$\textit{Equation 2:}\quad \boldsymbol{Q(t) = 1 - exp\left(-\left(\frac{t}{\tau}\right)^{\gamma}\right)}$$

Regarding the circuit model, the Quench Factor was implemented using a basic ABM block component, outputting a value which was then subsequently used in the calculation of electrical resistivity as mentioned in **Subsection 6.4.2**.

6.4 Construction of Model in DEHDL

6.4.1 Use of Analogue Behavioural Model Components

ABM components allow their characteristic properties to be defined as an expression of variables called from specific points within the circuit model. All of the components modelled had a specific equation programmed as its implementation. This allowed for the creation of, e.g. temperature dependent resistors and current dependent inductors [19]. However, it should be noted that these components must be either a controlled current source or a controlled voltage source. The following subsections will briefly describe how each electrical component was constructed using an ABM component.

6.4.1.1 Analogue Behavioural Model of a Resistance

An ABM component for a controlled current source which, using Ohm's Law (*Equation 3*) as its implementation, was used to model a resistor (see *Figure 18*). This was a viable option, as the calculated value for current generated by the source was applied negatively within the circuit. The inherent reduction in overall current flow would balance to the value which it would have been if a resistance of a given value was present. The parallel resistance shown is merely a non-physical, large resistance to assist simulation convergence.

Equation 3: $\boldsymbol{V(t) = I(t)R(t)}$

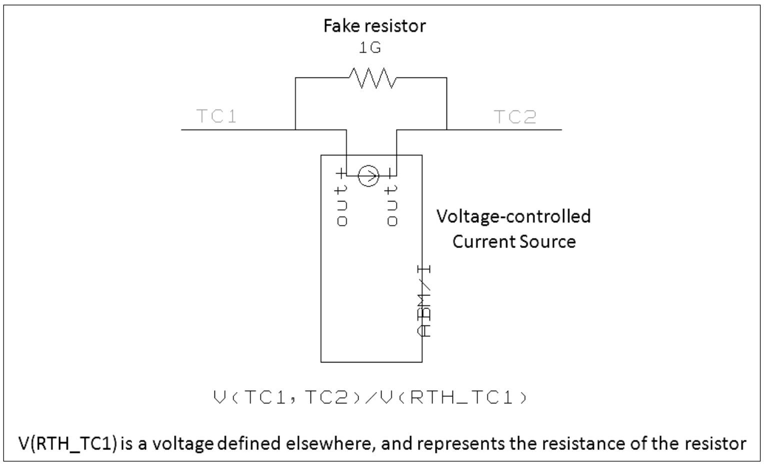

Figure 18: ABM Component modelling of a resitor [fig 5]

6.4.1.2 Analogue Behavioural Model of an Inductance

A similar construct (*Figure 19*), again shows an ABM component for a controlled current source, and the same non-physical parallel resistance. However, the input equation (*Equation 4*), set as the component implementation, is that of the current in an inductor. The current was applied in the same manner to reduce the overall current flow to the value which it would have been if an inductance of a given value was present.

$$\text{Equation 4:}\quad \boldsymbol{I(t) = \int_0^{\infty} \frac{\Delta V_{mag}}{L_{mag}} dt}$$

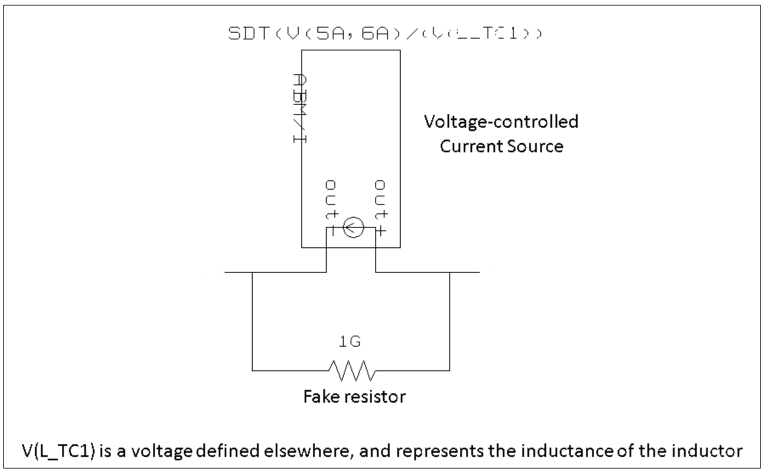

Figure 19: ABM Component modelling of an Inductor [fig 5]

6.4.1.3 Analogue Behavioural Model of a Capacitor

The chosen method of capacitor model (*Figure 20)* differed from that of the resistor and inductor models due to convergence issues (see **Appendix A.5**). The model used two basic ABM block components, summed using a voltage-controlled voltage source. One of the ABM components was merely set to zero while the input for the other was the voltage equation for a capacitor (*Equation XXX*). The voltage-controlled voltage source was then given a gain of -1 to simulate a reduction in voltage equivalent to that which a capacitor of the calculated value would cause.

$$\textit{Equation 5:}\quad \boldsymbol{\Delta V(t) = \int_0^{\infty} \frac{I_{mag}}{C_{mag}} dt}$$

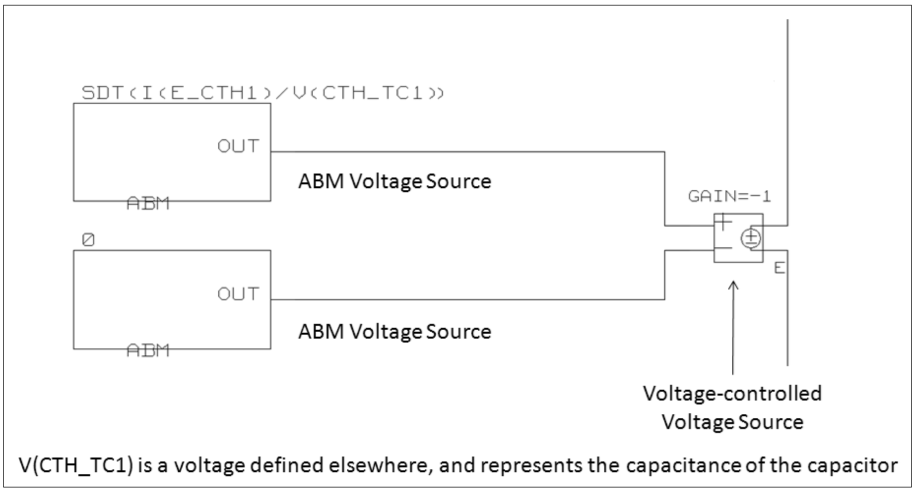

Figure 20: ABM Component modelling of a Capacitor [fig 5]

6.4.1.4 Analogue Behavioural Model Expressions

Use of basic, not current or voltage source, ABM components allowed the ability to calculate a value based on general expressions, functions and operators. This allowed for the implementation of complex equations within the circuit model and this ability was commonly sighted throughout the bulk of the components of the electro-thermal model.

6.4.2 Use of ABM Components for the Calculation of Manually Implemented Equations

The following subsections detail the processes used for the calculation of parameters which require manually implemented equations. This was mostly done with the use of basic ABM block components, entering the equations as their implementation. An example of an entered implementation, specific to the calculation of electrical resistivity, is shown below:

LIMIT((1.7/RRR_CU_MQXx+1/(2.33G/V(%IN)**5+957K/V(%IN)**3+163/V(%IN)))*10N+(0.37+500U*RRR_Cu_MQXx)*0.1N*V(B_Qx),113.333P,9.999G)

The LIMIT(x,y,z) function is merely a dictation of boundaries so that the calculated value for 'x' never went below value 'y' or above value 'z'.

6.4.2.1 Calculation of the Electrical Resistance of the Magnet Coils

The electrical resistance was calculated for each coil, taking into account four major aspects: the electrical resistance of copper **(Cu)** in its normal state; the electrical resistance of Cu in its superconducting state; the electrical resistance of Niobium-Titanium **(NbTi)** in its normal state; and the electrical resistance of NbTi in its superconducting state. These values were calculated using a rearranged version of the basic resistivity equation (*Equation 1*).

For both states of NbTi, a constant value of resistivity, from industry standard values, was used. These were 560nΩm for NbTi in its normal state and 0.1aΩm in its superconducting state. The resistivity of Cu, in its superconducting state was negated (0Ωm), but in its normal state, the value was calculated taking into account the current temperature of the cable, the magnetic field strength of the magnet and the magnet's residual resistivity ratio (**RRR**). The RRR (*Equation 6*) is defined as the ratio of resistance at normal state temperatures (293K) to the resistance at superconducting state temperatures (1.9K) [20]. The resistivity was then calculated according to *Equation 7*.

Equation 6: $$\boldsymbol{RRR_{mag} = \frac{\rho_{293K}}{\rho_{1.9K}}}$$

Equation 7: $$\boldsymbol{\rho_{Cu,thermal} = 0.37 + \left(\frac{1.7}{RRR_{mag}} + \frac{1}{\left(\frac{2.33G}{T_{cable}{}^{5}}\right)+\left(\frac{957k}{T_{cable}{}^{3}}\right)+\left(\frac{163}{T_{cable}}\right)}\right)n + \left(\frac{500\mu}{RRR_{mag}} \times B_{mag}\right)0.1n}$$

After each resistivity value was calculated, they were then input into subsequent ABM components and multiplied by the dimensions of the cable, in order to acquire a corresponding value for electrical resistance. These resistance values, for both superconducting and normal states, were then multiplied separately, as if in parallel, using the equation for resistors in parallel (*Equation 8*).

Equation 8: $$\boldsymbol{\frac{1}{R_{tot}} = \frac{1}{R_{Cu}} + \frac{1}{R_{NbTi}}}$$

Finally, the now accurate electrical resistance values, for both superconducting and normal states, were multiplied by what has been termed the 'Quench Factor' (detailed in **Subsection 6.4.4**) and subsequently summed together (*Equation 8*) to acquire the magnet coil's electrical resistance.

Equation 9: $$\boldsymbol{R_{tot,electrical}(t) = \Big(\big(\rho_{Cu,NSC} + \rho_{Cu,SC}\big)Q(t)\Big) + \Big(\big(\rho_{NbTi,NSC} + \rho_{NbTi,SC}\big)Q(t)\Big)}$$

6.4.2.2 Calculation of the Thermal Resistance of the Magnet Coils

Thermal resistance takes into account the cable temperature, the electrical resistivity of Cu in its normal state and the cross-sectional area of the cable. The thermal conductivity was calculated, for each coil, using the *Equation 10*:

$$\textit{Equation 10:}\ \boldsymbol{\sigma_{Cu,thermal} = \frac{T_{cable}}{\rho_{Cu,thermal}} \times 24.5n}$$

The calculated values were then inverted to acquire values for thermal resistivity and were then subsequently multiplied by the cable's cross-sectional area to give values for thermal resistance as follows (*Equation 11*).

$$\textit{Equation 11:}\ \boldsymbol{R_{thermal} = \frac{1}{\sigma_{Cu,thermal}} \times W_{mag}}$$

It should be noted that in the model this calculation is only taken into account if a non-adiabatic simulation is desired. The option to choose between adiabatic and non-adiabatic simulations was implemented with the inclusion of an 'adiabatic flag'.

6.4.2.3 Calculation of the Thermal Capacitance of the Magnet Coils

Calculating the thermal capacitance involved most of the components included in the electro-thermal model. This was due to the varying equations used for thermal capacity at specific temperature values. Subsequently, for any calculated cable temperature, the specific variation of equation for thermal capacity was called.

Following the calculation of the thermal capacity values for each coil, the sum of the Cu and NbTi thermal capacities were multiplied by the corresponding ratio (Cu/NbTi) and finally the thermal capacitances were calculated as shown below (*Equation 12*).

$$\textit{Equation 12:}\ \boldsymbol{C_{thermal} = \left(\left(\frac{\frac{Cu}{NbTi}}{\frac{Cu}{NbTi}+1}\right) Q_{Cu} + \left(\frac{Cu}{NbTi}\right) Q_{NbTi}\right) \times \frac{\pi {D_{cable}}^2}{4N_S L_{cable}}}$$

6.4.2.4 Calculation of the Thermal Resistance of the Insulation layer of the Magnet Coils

Surrounding the metals of a magnet coil's wire is a layer of insulation made from a polymide, KAPTON®, which is stable at a wide range of temperatures (0-130K) [21]. This insulation layer should be taken into account during non-adiabatic simulations. Thermal conductivity was calculated according to

Equation 10, using properties and temperature of the insulation layer, and was then subsequently multiplied by the cable thickness and the inverse was taken to produce a value for thermal resistance (*Equation 11*).

6.4.2.5 Calculation of the Difference in Cable Temperature of the Magnet Coils

The difference in cable temperature, following a quench, is calculated according to *Equation 13*, seen below. The corresponding design schematic is shown in **Appendix E.4**.

Equation 13: $$\Delta T_{cable}(t) = T_{cable}(t) - T_{cable,1.9K} = \frac{\left(P_{thermal}(t) - \frac{d}{dt}(C_{thermal} \times \Delta T_{cable}(t))\right)}{R_{thermal,cable} + R_{thermal,ins}}$$

Equation 14: $$P_{thermal}(t) = I_{coil}(t) \times R_{tot,electrical}(t)$$

It involves taking into account the ohmic power (*Equation 14*), the thermal resistance of the cable (*Equation 11*), the thermal capacitance of the cable (*Equation 12*) and the thermal resistance of the cable's insulation layer (see **Subsection 6.4.2.4**).

6.4.2.6 Calculation of the Magnetic Field produced by the Magnet Coils

The magnetic field was calculated taking into account the magnetic transfer function of the magnet. The integrated transfer function was acquired, for each magnet, by analysing graphs, which included the transfer function, in relation to current level. The magnetic field was then derived according to the following *Equation 15*.

Equation 15: $$B_{mag}(t) = I_{mag}(t) \times TF_{mag}$$

6.4.2.7 Calculation of the Magnet's Inductance

It is known that, with respect to current, the inductance of an electromagnetic coil, though linear at low and mid ranges, reduces as current reaches the maximum levels permissible by the mechanical properties of the coil's material. This was taken into account by the simple multiplication of the ratio transfer function with the maximum value for inductance. Regarding the final ITS circuit model in particular, no tests of this relation for the magnets were made by the manufacturers and thus could not be taken into account. Therefore, the magnet's inductance was assumed to be linear throughout.

6.4.3 Electro Thermal Model of a Single Magnet as constructed in DEHDL

The final electro-thermal model of a magnet, as constructed in DEHDL, can be found in **Appendix E.5**.

6.4.4 Separately Modelling a Magnet's Inner and Outer Coils

Table 2 and *Table 3* show that the parameter values of the inner and outer coils of each magnet vary. The difference was deemed great enough to justify the separate modelling of the inner and outer coils of each magnet. In testing this, the results, when compared to modelling the full magnet coil as a whole, proved more accurate, so the decision was made that separate modelling, though computationally taxing, was the better option for the final model design. The full design schematic, as well as specific calculation components, can be found in **Appendix E.7**.

6.4.5 Final Parameter List

As mentioned in **Section 4.4**, the circuit model utilises the DEHDL's parameter list option. The final list of parameters, as constructed in DEHDL, can be found in **Appendix E.8**.

6.5 Problems Encountered

Throughout the development of the electro-thermal model, the main problems encountered were: the accurate referencing of specific components/areas of the circuit, due to the scale and complexity of the model; the need for re-evaluation of how specific components were modelled; and the convergence errors present when simulating, which required constant revision and extensive debugging.

7 FINAL MODEL SIMULATION RESULTS

7.1 Confirmation of the Accuracy of Simulation Results

Regarding the level of accuracy, it was specified, by the contractor, that simulation results were to fall within an error of 1% or less, when compared with the LHC's PM data. The following subsections detail some of the most important comparisons made, showing the results and the model's accuracy during common events. These include an FPA and quenches in both ITS circuit types. Randomly chosen for the simulations detailed in this section, were the RQX.L8 (Type 2) and the RQX.L5 (Type 1) systems.

7.1.1 Analysis of the Accuracy of Current and Voltage levels when simulating an FPA

7.1.1.1 RQX.L8, PNO.D11 Test, Current Analysis following a FPA

The following plot (*Figure 21*) is the direct comparison of simulation data and measurements physically recorded in the LHC, during the PNO.D11 commissioning test of the RQX.L8 circuit on 18/11/09. The simulation data is that which was produced when running simulations of the aforementioned test with the final circuit model. *Figure 21* specifically details the rate of change of current levels within the circuit with respect to time flowing through the two main RQX.L8 and RTQX2.L8 PC current loops.

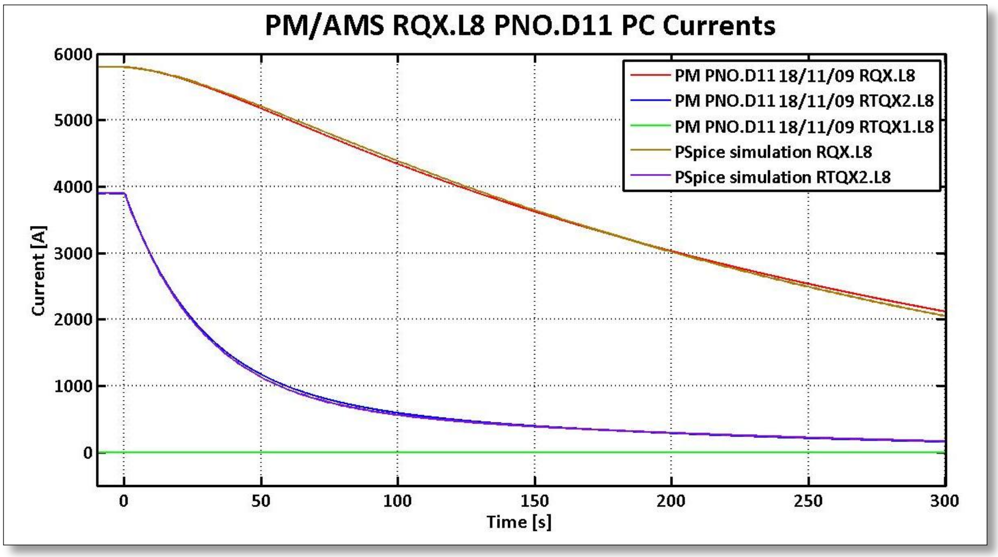

Figure 21: Plot of comparison, of rate of change of current, between AMS and LHC data for commissioning test PNO.D11 on circuit RQX.L8. 100% current, 2 main PCs active, RTQX1 off, FPA @ t=0.

In this test an FPA was initiated at time = 0. The resultant curve showed a slow (>400s) exponential decay of current due to the discharge and subsequent dissipation of the energy stored in the magnets.

From the plot, it is clearly shown that the simulation data followed the same characteristics as the measured data and did so to within an accepted tolerance. It is thought that the main causes for inaccuracies in this test were minor differences in the diode characteristics, generated in the AMS model editor.

7.1.1.2 RQX.L8, PNO.D11 Test, Voltage Analysis following a FPA

The following plot (*Figure 22*) the direct comparison of simulation data and measurements physically recorded in the LHC, during the PNO.D11 commissioning test of the RQX.L8 circuit on 18/11/09. The simulation data is that which was produced when running simulations of the aforementioned test with the final circuit model. *Figure 22* specifically details the rate of change of voltage levels within the circuit with respect to time as measured across the terminals of the RQX.L8 and RTQX2.L8 PCs.

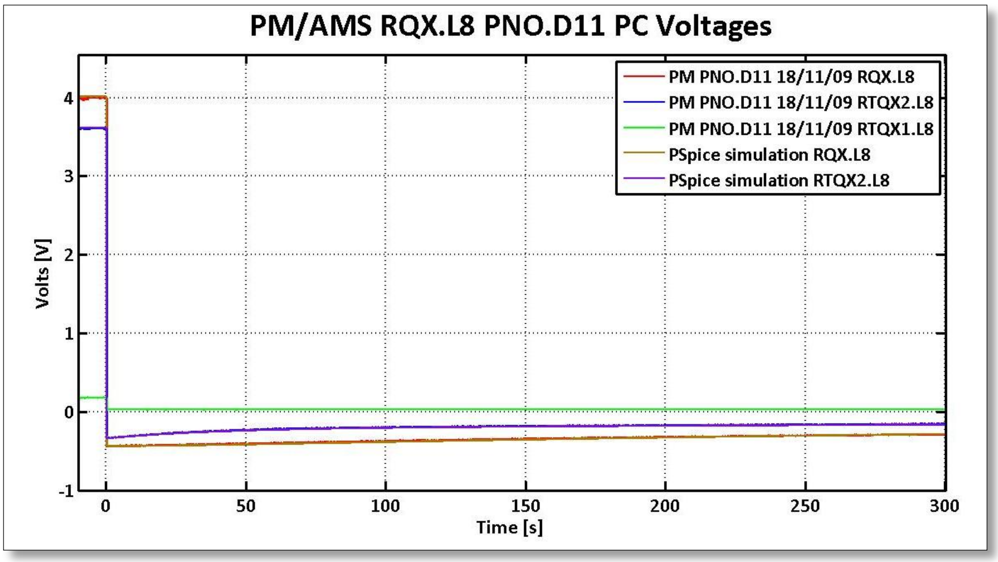

Figure 22: Plot of comparison, of the rate of change of voltage, between AMS and LHC data for commissioning test PNO.D11 on circuit RQX.L8. 100% current, 2 main PCs active, RTQX1 off, FPA @ t=0.

In this test an FPA was initiated at time = 0. The resultant curve showed a sudden change in potential across the PCs resulting in a slowly reducing (>400s) negative voltage corresponding to the discharge and subsequent dissipation of the energy stored in the magnets. From the plot, it is clearly shown that the simulation data followed the same characteristics as the measured data and did so with impressive accuracy. It is thought that the main causes for the remaining minor inaccuracies in this test were, again, minor differences in the diode characteristics, generated in the AMS model editor.

7.1.2 Analysis of the Accuracy of Current and Voltage levels when simulating FPA

7.1.2.1 RQX.L8, PLI3.f6 Test, Current Analysis following a Quench

The following plot (*Figure 23*) is the direct comparison of simulation data and measurements physically recorded in the LHC, during the PLI3.f6 commissioning test of the RQX.L8 circuit on 16/06/08. The simulation data is that which was produced when running simulations of the aforementioned test with the final circuit model. *Figure 23* specifically details the rate of change of current levels within the circuit with respect to time flowing through the two main RQX.L8 and RTQX2.L8 PC current loops as well as the now-opened FWT/FWD current loops.

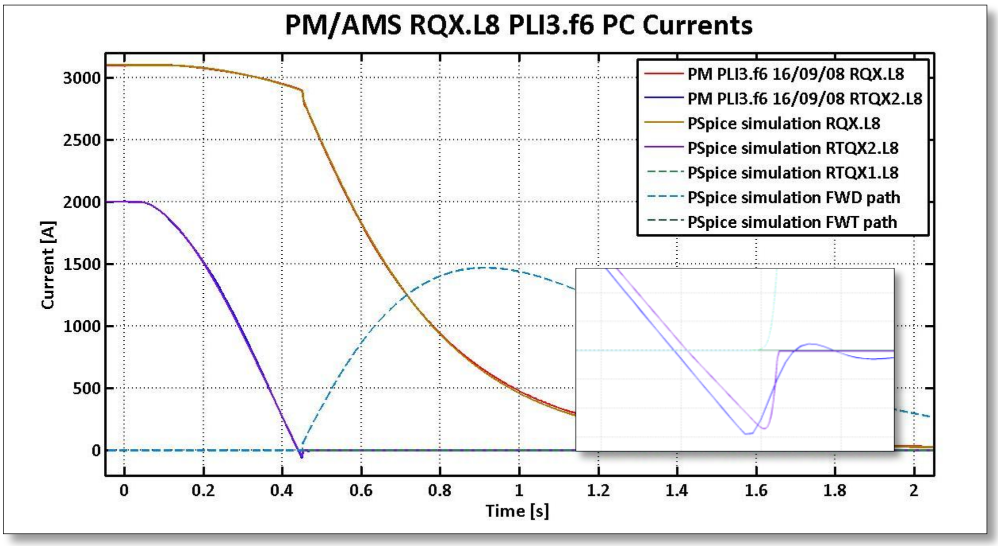

Figure 23: Plot of comparison, of the rate of change of voltage, between AMS and LHC data for commissioning test PLI3.f6 on circuit RQX.L8. 50% current, all 3 PCs active, RTQX1 positive, Quench @ t=0.

In this test the quench of a magnet and subsequent firing of the heaters was simulated at time = 0. The resultant complex curve is the quick discharge (< 3s) of stored energy within the magnets. The level of accuracy proves that, not only did the circuit model have accurately implemented parameters, but it calculated the electrical and thermal properties, as well as estimating the quench propagation velocity, exceptionally well. Also noteworthy, is the model's ability to accurately simulate the transition of current, initially flowing in the RQX and RTQX2 current loop, to the RQX and now-opened FWT and FWD current loops. A close up of this transition is included in *Figure 23.*

7.1.2.2 RQX.L8, PLI3.f6 Test, Voltage Analysis following a Quench

The following plot (*Figure 24*) is the direct comparison of simulation data and measurements physically recorded in the LHC, during the PLI3.f6 commissioning test of the RQX.L8 circuit on 16/06/08. The simulation data is that which was produced when running simulations of the aforementioned test with the final circuit model. *Figure 24* specifically details the rate of change of voltage levels within the circuit with respect to time as measured across the terminals of the RQX.L8 and RTQX2.L8 PCs.

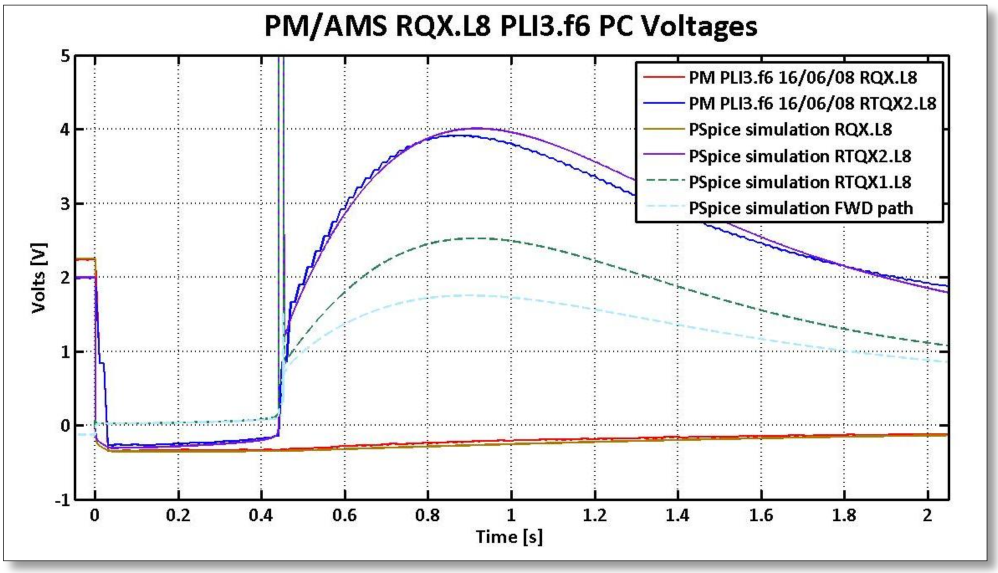

Figure 24: Plot of comparison, of the rate of change of voltage, between AMS and LHC data for commissioning test PLI3.f6 on circuit RQX.L8. 50% current, all 3 PCs active, RTQX1 positive, Quench @ t=0.

It follows, since the current analysis was impressively accurate, that the voltage analysis would also be relatively accurate. The plot shows that for the initial, and most important, stage of the quench the model proved exceptionally accurate when compared with recorded data. The simulation followed the rate of change of voltage very closely even during the transition stage, with the exception of voltage 10ms spike. It is also noteworthy that the rate of change of voltage across the RQX PC is that which is determined by the estimation of the quench propagation velocity function. It is thought that apparent differences in potential, across the RTQX2 PC, are due to minor inaccuracies in the characteristics of the FWT and FWD, as no current is flowing through this path after the transition and the potential is merely the result of the difference between that of the FWT and FWD.

7.1.3 Proof of Accuracy when simulating FPA in both ITS circuit types

An important aspect of the project was to make the circuit model viable when used to simulate any of the eight ITSs, assuming local specific parameters were entered. This subsection includes an additional quench comparison for the circuit RQX.L5. This circuit is of a different type to that of RQX.L8.

7.1.3.1 RQX.L5, PLI3.f6 Test, Current Analysis following a Quench

The following plot (*Figure 25*) is the direct comparison of simulation data and measurements physically recorded in the LHC, during the PLI3.f6 commissioning test of the RQX.L5 circuit on 16/09/08.

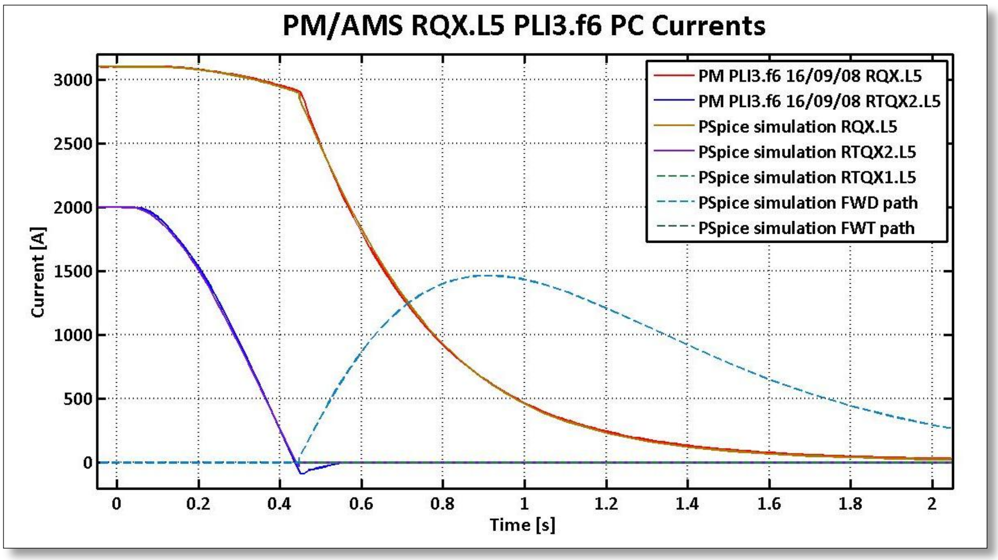

Figure 25: Plot of comparison, of the rate of change of voltage, between AMS and LHC data for commissioning test PLI3.f6 on circuit RQX.L5. 50% current, all 3 PCs active, RTQX1 positive, Quench @ t=0.

The comparison proves, that even with altered parameters specific to that of the RQX.L5 circuit, the model simulated recorded data to roughly the same accuracy. It is noteworthy that no manual parameter 'tweaking' was involved in this simulation.

7.2 Summation of Comparative Results

It is clear that the simulations carried out, using the final model, compare with recorded data to an exceptional accuracy. When an FPA or quench was simulated, comparative results fell comfortably within the specified <1% deviation, during the important stages of the transients. In fact, this circuit model proved, particularly when simulating a quench in the system, more accurate than previous models of other circuits. It is clear that the development of the circuit model, as a whole, had been very successful and that it was ready to be used for general circuit analysis and failure simulations.

8 Analysis of a Quench within the Inner Triplet System

8.1 Need for Analysis of a Quench within the Inner Triplet System

Even though a potentially dangerous event has not yet occurred since the start of operation of the LHC, it does not mean that it never will. With this in mind, the ability to simulate and analyse the system in operation is very useful, as the simulation can make important predictions concerning the stability and safety of the ITS during a variety of different scenarios, e.g. during normal operation; if a component defect is present; if a specific failure, e.g. the quench of a magnet, or number of failures, occur; theoretical worst case scenarios; or even when running at higher energy levels.

Due to the successful development of an accurate circuit model, full analyses, to a degree never done before, of most of the plausible events which may occur in the Inner Triplet System, can be easily made. This, in depth, form of analysis is made possible by utilising the AMS simulator's ability to plot any graph form, regarding any points within, or characteristics of, the circuit.

8.2 Full Analysis of 'Real-World' Quench Simulation

This section contains a detailed, but not exhaustive, analysis of a simulation programmed to be as close as possible to a plausible 'real-world' scenario of a quench occurring in the ITS, during normal operation. This scenario involves a quench in the system while all PCs are running stable at full current. Note that, in this case, the simulated event has not yet occurred within the ITS, and assumptions in parameter values, specifically those that scale with current, have been made without having direct data comparison for validity.

8.2.1 RQX.L8 – Quench@Full Current, All 3 PCs Active, RTQX1 Positive

This simulation corresponds to any event in which the QPS is triggered whilst operating at full current. This simulation is as close to a plausible 'real world' quench scenario as possible and thus the values of the resultant proposed figures, accounting for assumptions in current scaling parameters, are those that should be taken into account when questioning the safety and stability of the ITS, if this scenario were to happen.

8.2.1.1 Current Flow through Magnets

Figure 26 is a plot of the decay of the current flowing through each of the magnets. Firstly, it can be seen that the highest current level, flowing through the Q2a and Q2b magnets, prior to the point of the simulated quench (time < 0s), was that of the sum of the current produced by both the RQX and RTQX2 PCs (~9.5kA), due to the nested loop circuit design. Secondly, it can be seen that the Q1 and Q3 magnets were subject to current levels of that produced by the RQX PC (~6kA), with Q3 also receiving the additional current produced by RTQX1 (~400A), as the circuit type used was Type 2.

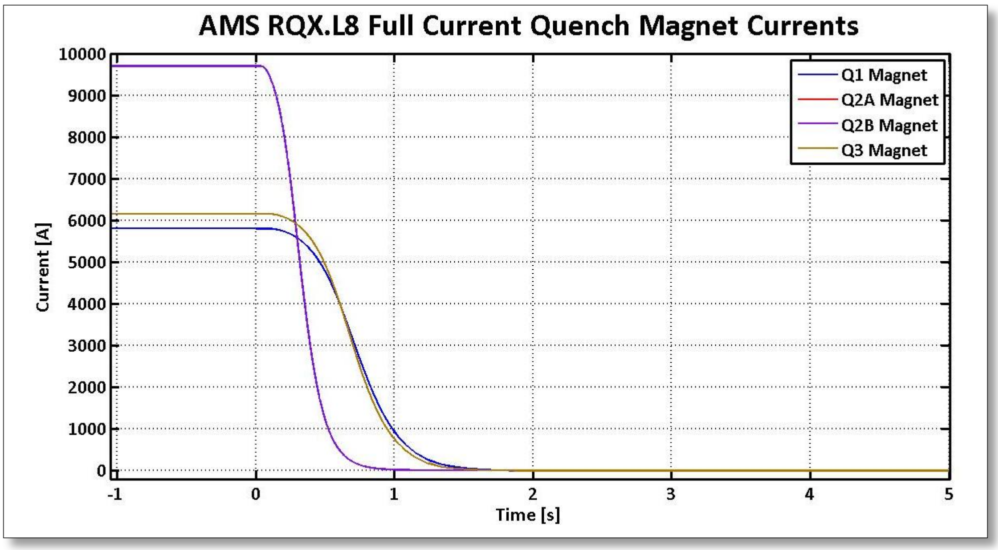

Figure 26: Plot of Current within the Magnet during a Full Current Quench Simulation

After the point of quench (time = 0s) when the PCs were shut off and the energy stored in the magnets were discharging, the current flowing through all magnets fell to zero in an expected exponential decay with an expected time constant of L/R.

8.2.1.2 Magnetic Field Strength

Figure 27 details the corresponding rate of change of the magnetic field strength, as calculated according to *Equation 15*. It can be seen that the MQXA magnets (Q1 and Q3), having a larger inductance than the MQXB magnets (Q2a and Q2b), produced a stronger magnetic field.

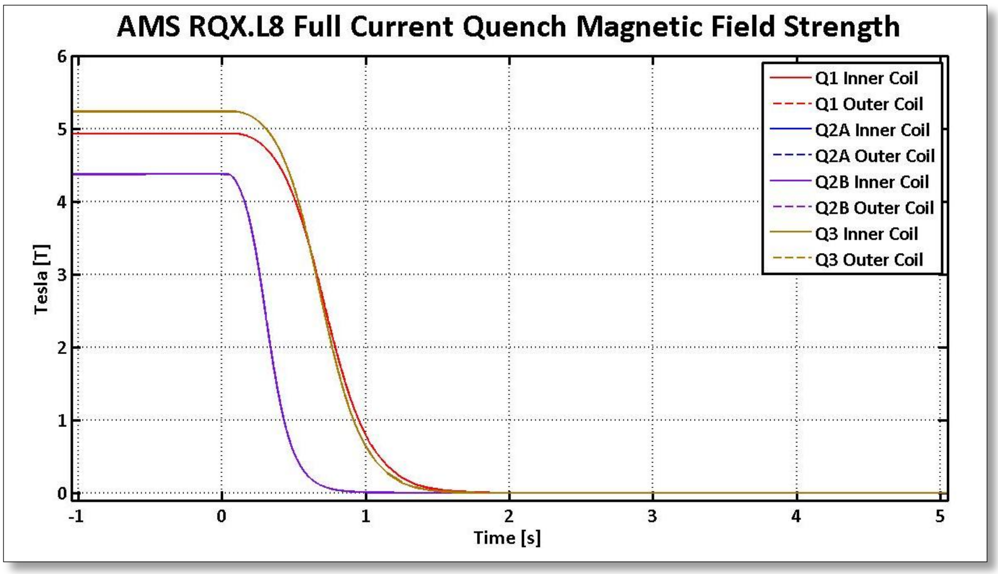

Figure 27: Plot of the Magnetic Field Strength in the Magnets during a Full Current Quench Simulation

It is also apparent that the, previously shown (*Figure 26*), additional current in the Q3 magnet further increased its magnetic field. As expected, there was no major difference in field between the inner and outer coils of each separate magnet.

8.2.1.3 Energy Stored in Magnets

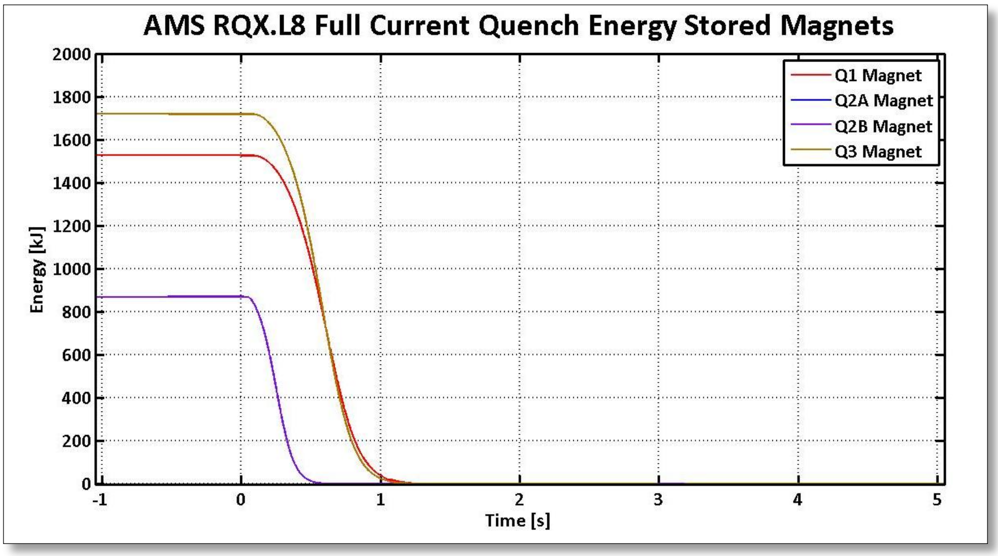

Figure 28: Plot of the Energy stored in the Magnets during a Full Current Quench Simulation

Figure 28 shows the energy stored in the magnets before and after a quench was simulated. It can be seen that prior to the quench, the energy stored, as calculated using *Equation 16*, was greater in the MQXA magnets because of their larger inductance, but only by approximately double, due it being proportional to the square of the current (larger in MQXB magnets). Again, magnet Q3 had an increase in stored energy above that of the Q1 magnet, due to the additional current produced by the RTQX1 PC.

$$\text{Equation 16: } E_{stored} = \frac{1}{2} L_{mag} I_{mag}$$

8.2.1.4 Energy Dissipated in Magnets

Figure 29 shows a plot of the amount of energy stored in the magnets which is then subsequently dissipated back across the magnets, following a quench.

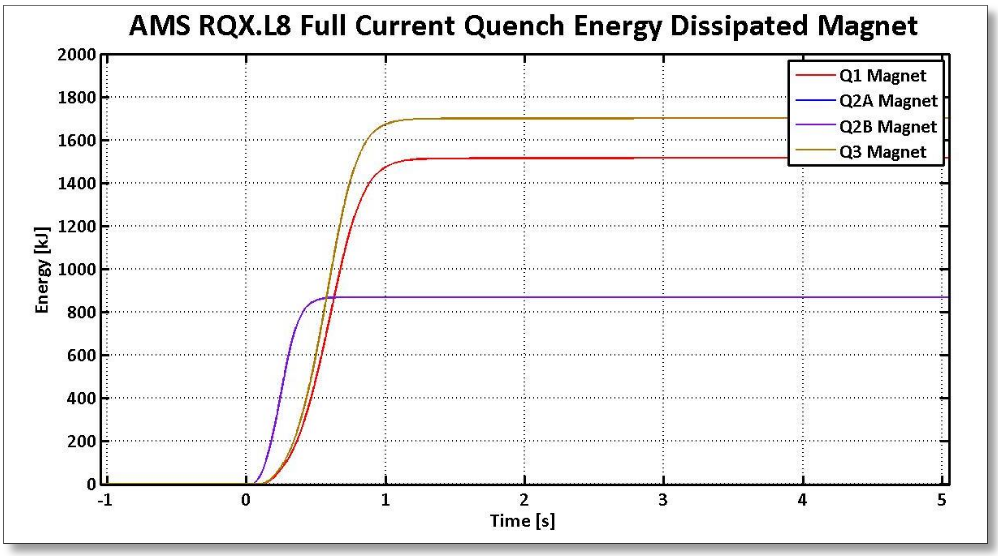

Figure 29: Plot of the Energy Dissipated in the Magnets during a Full Current Quench Simulation

This graph is particularly interesting in that the amount of energy dissipated in the magnets was in excess of 95% of the original stored energy. These results, justified by the calculated electrical resistance (see **Subsection 8.2.1.6**), proved worrying, because under this circumstance, if the system were to be running at a higher energy, the magnet could be permanently damaged. The energy dissipated in the magnets was calculated according to *Equation 17*.

$$\text{Equation 17: } E_{dissipated}(t) = \int_{t_{quench}}^{\infty} I_{mag} \Delta V_{mag} dt$$

8.2.1.5 Temperature of the Magnet Coils

Figure 30 shows a plot of the rate of change of temperature within each of the magnet coils before, during and after the quench.

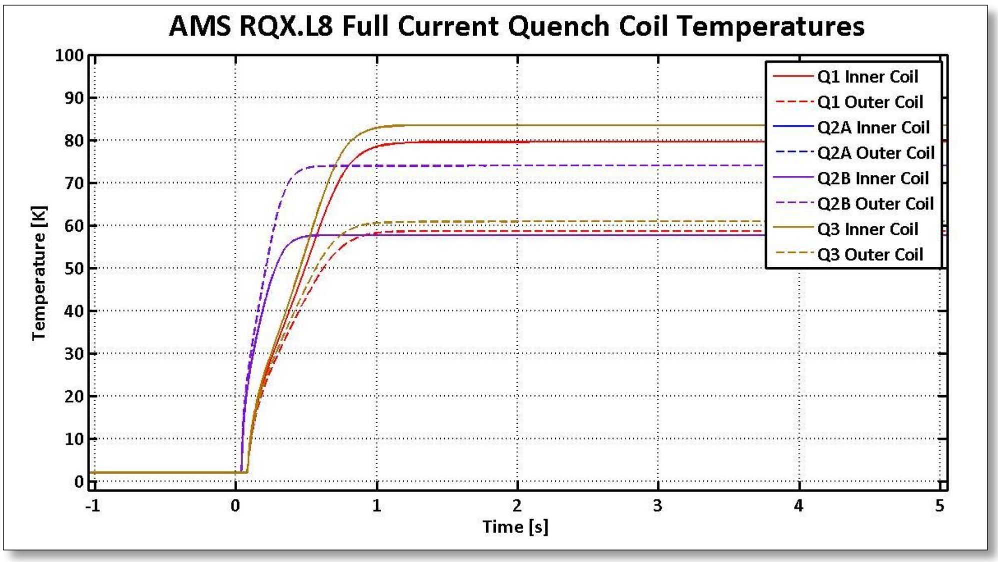

Figure 30: Plot of the Temperature within the Magnets during a Full Current Quench Simulation

It displays the non-linear increase in temperatures, which is generated in correspondence to the implemented non-linear Quench Factor (see **Subsection 6.3.2.1**). The final temperature in each coil is an acceptable value of 60-90K, differing for each coil due to mechanical properties and inherent thermal capacity, but the rate of the increase in temperature is worryingly fast and is worthy of further study.

8.2.1.6 Electrical Resistance of Magnet Coils

Figure 31 is a plot of the electrical resistance in the magnet coils, showing the transient characteristics of the rate of change of resistance of the magnet coil during a quench. It shows that after the point of quench, the resistances had a mostly linear transient, eventually saturating to the magnet's maximum resistance value, determined by its mechanical properties. This result is particularly interesting, as the increase in resistance was shown not to be directly proportional to the percentage of the magnet that was quenched with respect to time i.e. the Quench Factor.

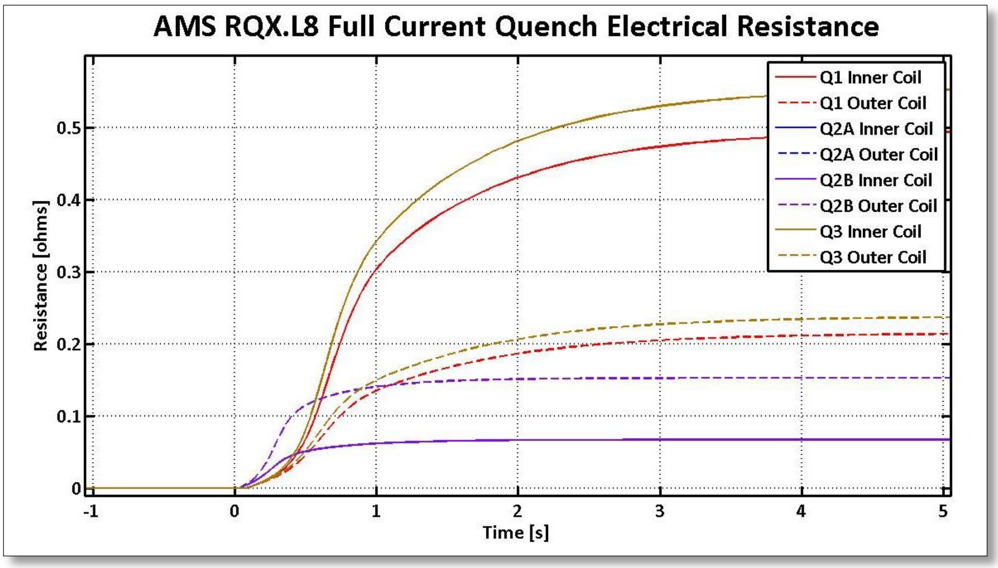

Figure 31: Plot of the Electrical Resistance of the Magnets during a Full Current Quench Simulation

It is also of note that the values of resistance, in the order of hundreds of mΩ, were much greater than that of the rest of the circuit, which amounted to only a few mΩ. This explains the previously observed dissipation of almost all of the stored energy in the magnets back across the magnets.

8.2.1.7 MIITs of the Magnet Coils

A magnet's MIITs (*Equation 18*) is a standard way of comparing the performance, stability and safety, during a quench, of a superconducting magnet, as it can be used to estimate the magnet's required minimum resistance and temperature limits for 'self-protection'. Self-protection negates the need for a dedicated energy extraction system, which prevents the stored energy dissipating in the magnets. The ITS has no energy extraction system, which means that the original design calculations and measurements, taken during the magnets' commissioning, predicted that the magnets had sufficient natural electrical resistance in normal state for 'self-protection'. *Figure 32* shows a plot of the MIITs of the magnet during the simulated quench.

Equation 18: $$\int_{t_{quench}}^{\infty} I_{mag}^{2} = 10^{6} MIITs - \int_{0}^{t_{quench}} I_{mag}^{2}$$

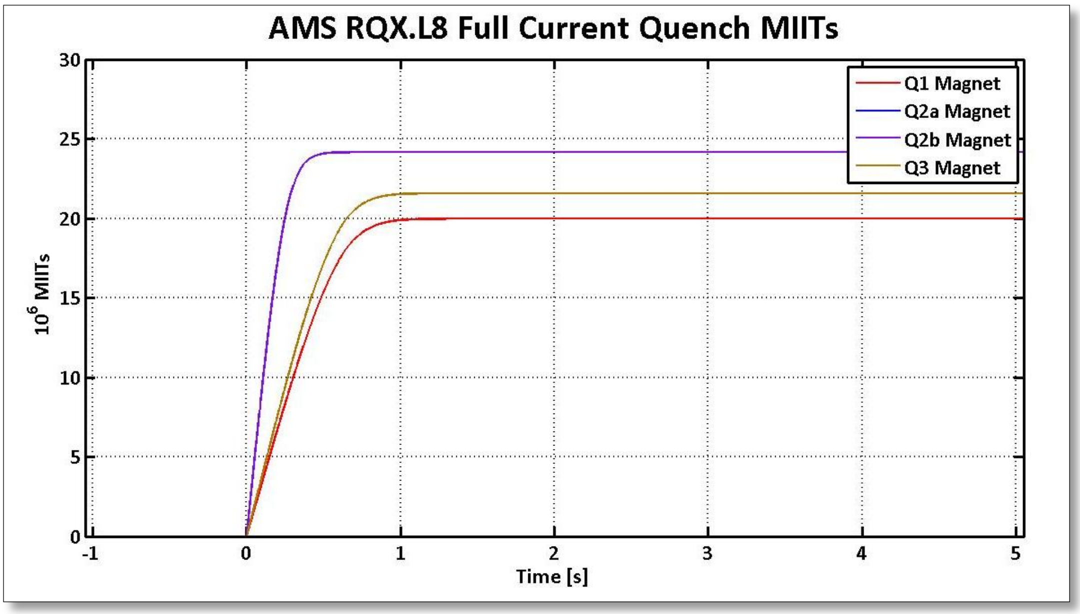

Figure 32: Plot of the generated MIITs of the Magnets during a Full Current Quench Simulation

The results proved worryingly high. To put the MIITs values into perspective, other quadrupole magnet circuits produce ~5-10x10^6 MIITs during a quench. In this case, further analysis was called for.

The calculation of the minimum effective resistance required for self protection was done according to the following equation (*Equation 19*).

$$\textit{Equation 19:} \quad R_{eff,min} = \frac{{I_{mag}}^2 L_{mag}}{10^6 MIITs - \int_0^{t_{quench}} {I_{mag}}^2}$$

The results of the calculations and the corresponding electrical resistance (see *Figure 31*) of each magnet, is shown in *Table 6*.

Table 6: Comparison of calculated minimum safe resistance with actual electrical resistance

Min Safe Resistance	Electrical Resistance	
70	~200	mΩ
158	~700	mΩ

The results shown confirmed that, during a quench, the electrical resistance of the magnet was higher than the calculated minimum to 'self-protect'. This proved, though originally thought otherwise, that the MIITs of the magnets of the ITS in this circumstance were of acceptable values, and suggested that the QP velocity, as accelerated by the magnets' quench heaters, was fast enough to ensure the 'self-protection' of the magnets.

8.2.2 Summation of 'Real-World' Quench Analysis

The analysis, which was carried out, showed some very interesting results. The fact that almost all of the energy stored in the magnets was then subsequently dissipated back across the magnets, gave rise to the questioning of the original design of the system. Furthermore, the magnets' MIITs values of up to $25x10^6$ MIITs were shown to be much higher than expected (almost double). It was, however, proven in further analysis that the quench heaters of the ITS successfully propagate the quench fast enough, allowing magnets to 'self-protect', ensuring the stability and safety of the system as a whole.

8.3 Simulation of 'Real-World' Quench with Component Defects/Failures

Establishing that a system is safe and acting as expected, during common and even some uncommon events, is very important, but to further investigate the system's stability, simulations can be done with a theoretical worst case scenario or with hypothetical failures throughout the circuit. This section investigates the results of simulations in which errors/failures in the system have been forced/manually implemented. These include, e.g. the failure of a thyristor triggering, and a short within a magnet coil. All scenarios are simulated during a quench at full current.

Again, it should be noted that the following scenarios, as yet, have never occurred in the LHC and thus, no direct comparison can be made for full confirmation of the validation of the simulation results. Therefore, assumptions of parameters that scale with current were made.

8.4 Simulation of a Short-to-Ground in Magnet Coils

With the simple inclusion of a temporary path from a magnet's inductor to ground via a variable resistance, it is possible to test if a short-to-ground would have any problematic characteristics other than a minor reduction in inductance. During these simulations, it was important to include the system's resistor, found to be 100Ω, in its ground path.

Using the AMS simulators' parametric sweep analysis, it was easy to see if a short resistance value, within a plausible range (0.1Ω-100Ω), would produce any significant effect.

8.4.1 Q1 Magnet Short-to-Ground Parametric Sweep Analysis

Shown below (*Figure 33*) are the parametric sweep results of values 0.1Ω - 100Ω. It is, however, apparent that this scenario is safe, with negligible effect, due to the circuit's deliberately large 100Ω ground resistance.

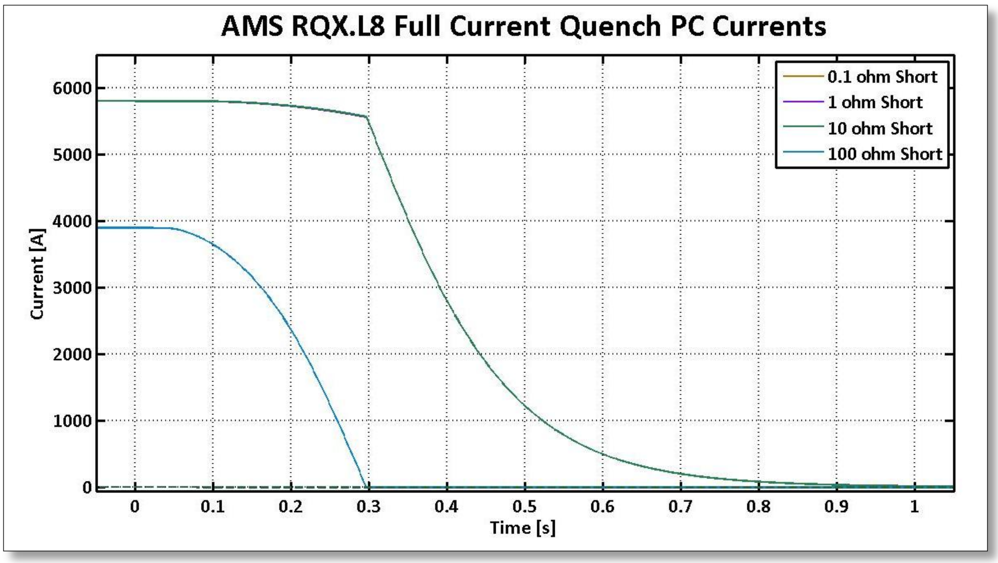

Figure 33: Plot of Parametric Sweep of short-to-ground resistance values, simulating a short present in the Q1 magnet during a Full Current Quench Simulation

8.4.2 Q2 Magnet Short-to-Ground Parametric Sweep Analysis

Running the same type of simulation, with the variable resistor to ground placed from the Q2 magnet, also produced no major change in the circuit's stability.

8.4.3 Q3 Magnet Short-to-Ground Parametric Sweep Analysis

Following the same procedure, the test was run with the short simulator from the Q3 magnet. The results, again, showed no major changes.

8.4.4 Summation of Short-to-Ground Analyses

The short-to-ground analyses clearly showed that, as long as the circuit's intended ground resistance is in place, a short-to-ground from any of the magnets poses no major problems to the operation, or stability, of the system. From these results, it can be understood that, though not immediately threatening, a short-to-ground could be potentially difficult to diagnose.

8.5 Failures Regarding the FWT/FWD

During a quench, as shown in **Subsection 7.1.2.1**, a large percentage of the stored energy in the magnets is dissipated in the FWT/FWD loops. This section looks at the potential problem of the failure to trigger the FWT and the plausible scenario of faulty FWDs.

8.5.1 Failure to Trigger Free-Wheel Thyristors

A simulation was run in which, on detection of a quench by the QPS, there was a failure to trigger the thyristors of the FWT.

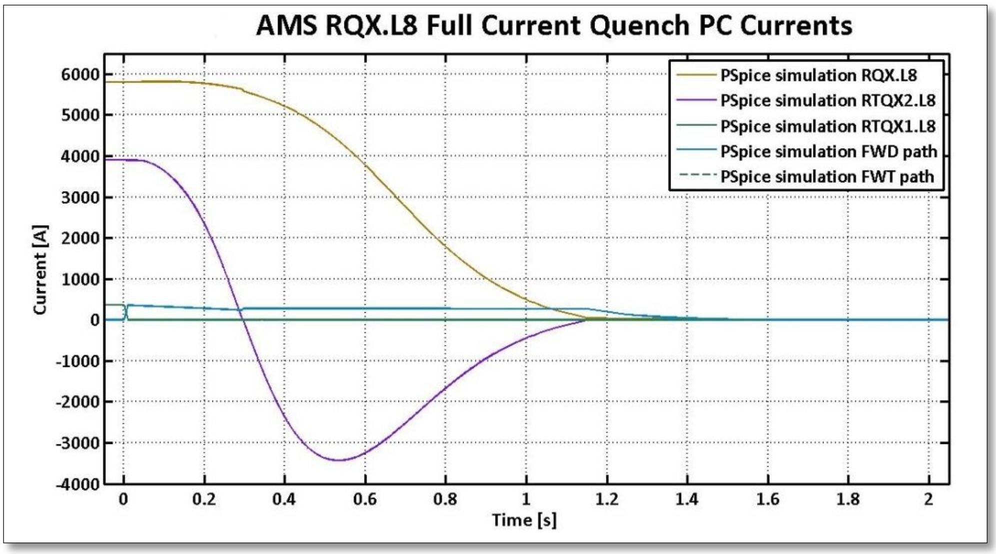

Figure 34: Plot of a Full Current Quench Simulation where the FWT has failed to trigger.

The result, shown in *Figure 34,* was that the RTQX1 PC's crowbar thyristors were forced to accept their maximum current flow and that, for the most part, the RTQX1 path was blocked, resulting in the RTQX2 diodes being forced into a reverse breakdown state, allowing for the catastrophic misdirection of very large current (~3.5kA), flowing down the RTQX2 diode path in reverse bias. The RTQX2 PC diode block has 20 diodes in parallel resulting in each diode having a reverse bias current of ~180A and a corresponding potential of ~4V. The diodes are, however, rated at 240A so the diodes should not falter during a quench.

8.5.2 Free-Wheel Diode Short-Circuit Test

As predicted, due to the nature of semiconductors reducing resistance with an increase in temperature and the normal resistance of the diodes being relatively close to zero, the short-circuit test produced similar results to that of normal quench tests. This is, however, non-physical as the temperature and pressure would eventually cause the FWDs to explode resulting in an open-circuit scenario.

8.5.3 Free-Wheel Diode Open-Circuit Test

A further simulation regarding the FWD was run to simulate the components' path as an open-circuit. The current remaining in the circuit, after the point of a quench, which should have safely flown through the FWD current loop, is now forced to flow down the RTQX2 diode block path resulting in the same reverse breakdown scenario of the FWT failure simulation.

8.5.4 Summation of Failure Simulations regarding FWT/FWD Analyses

It is clear from the failure simulations that the FWT and FWD paths are both a necessity within the system. Without them, or with the failure of either of them, a potentially dangerous scenario occurs. This could damage the diodes in parallel to the RTQX2 PC, and if more than 5 diodes are damaged and the reverse bias current exceeds the maximum rated current in all the remaining diodes, a very dangerous misdirection of the remaining energy would occur.

8.6 Summation of Component Defects/Failure Analyses

In simulating a quench scenario with the presence of failures or defects in the system, interesting results were found. As illustrated, the presence of a short-to-ground within any of the magnets would be safe, with no noticeable effect because of the system's design ground resistance. However, in simulating the failure of the vital FWT/FWD components, catastrophic misdirection of current was present. These currents, though within the diodes' rated values, could be potentially dangerous. Therefore, in light of these results, further analysis of these plausible circumstances is called for.

9 Conclusion

The specified aims of the project were: the designing of a circuit model of the ITS, capable of accurately simulating the electrical and thermal transients following the quench of a superconducting magnet coil within the system; and the subsequent use of the model to simulate and analyse the stability and safety of the system under this potentially dangerous scenario.

The designed, and successfully constructed, circuit model can, indeed, simulate the occurrence of a quench within the system and does so within the specified accuracy tolerance levels, as illustrated in the comparative analysis of simulation data with that of recorded data from the LHC. The model also has the ability to simulate a number of other failure scenarios, e.g. an FPA, an SPA, a failure in the QPS, defective components, short-to-ground analyses, and higher energy levels than that presently used at the LHC.

There are, however, inaccuracies still present in the model simulations, due to the limitations of the AMS model editor and of available component parameter information. The circuit modelling software was found to be somewhat tedious, and due to the complexity of the model, resulted in it not being particularly 'user-friendly'. Regarding the ability to simulate a variety of different scenarios, however, the final version of the circuit model could be improved upon, as it is still subject to an array of convergence issues.

The most important finding of the, aforementioned, analyses is the confirmation that if a quench were to occur within the Inner Triplet System of the Large Hadron Collider, when it is running at near maximum current, the magnets would 'self-protect' from damage and the system would remain stable.

In conclusion, it is evident from the accuracies of the comparative analyses that the specified aims were all successfully achieved. They also confirm that DEHDL software can, indeed, be used to adequately model the electrical and thermal transients following a quench in a high energy, complex powering system, containing superconducting magnets. It follows that the circuit model is now available for future use, when attempting to understand unexplained events occurring within the system or, for the prediction of the stability and safety of the system under further theoretical or hypothetical scenarios.

10 RECOMMENDATIONS FOR FURTHER WORK

- **Removal/reduction of convergence errors**

  This, I would say, is the most important recommendation regarding the circuit model itself as, without manual alteration of the circuit model, for each simulation, it is still subject to convergence errors, which will make using it troublesome for someone who is unfamiliar with the software.

- **Use of the circuit model to further simulate failure scenarios**

  There are several potentially dangerous scenarios which have yet to simulated. I would advise the construction of an exhaustive list followed by and the simulation and detailed comparative analyses of these listed scenarios.

- **Use of the circuit model to help find system energy limits**

  The simulations carried out so far have proven that, at current energy levels, the system is stable. I believe it would be interesting, and worthy the time, to simulate and analyse the point at which the system is no longer stable.

- **Development of circuit upgrades, if necessary, for system stability at higher energy levels**

  It is being planned that the energy levels of the LHC will be increased within in the next few years. If the results of the recommended simulations of the circuit being run at higher energy levels, proved the system to be unstable, the circuit model could be used to help redesign, or develop an upgrade for, the system.

11 Reflection

In reflecting on both the course and outcome of the project and the experience gained while working for an internationally renowned research organization, I am aware that, with regard to the former, I have added little to current engineering knowledge, let alone contributed to the ground-breaking aims of CERN. I am also conscious of the fact that my project results would not have been as successful, had it not been built-upon the extensive work of my predecessors.

Success of Project

Overall, I believe the project to have been a success. The aims of the project were all completed, within the given deadlines, and I am particularly proud of the level of accuracy of the simulations.

Self-Progression as a Professional Engineer

Throughout the duration of the placement, I believe that I have developed my skills as a professional engineer quite considerably, as well as having become more confidence in my ability.

Problems Encountered

A number of stressful weeks arose, where progression was held back as a result of the problems which were encountered. I am, however, proud of my perseverance, eventually managing to overcome all main difficulties.

What would I have done differently?

In hindsight, the main aspect of my work, which I would have done differently, would have been to be better organised. As being disorganised, on several occasions, led to a few inconveniences e.g. missing files, the odd unedited presentation or report. I would have also taken more time to understand the fundamentals and underlying physics behind the equations for calculations of the electro-thermal model, as I believe my knowledge in this area could be better.

Finally, I would like to reiterate my gratitude to those who allowed me such an incredible opportunity, who welcomed me on site and who advised/guided me throughout my time at CERN. My colleagues were all patient, understanding and wonderful to work with.

I am honoured to have been through, and will always cherish, this life-changing experience.

Thank You

Picture of myself, proudly alongside fellow technical students and John Ellis FRS, at CERN, on the day of the faster-than-light neutrinos seminar.

REFERENCES

Text references

[1] University of Glasgow, *Course Catalogue: Industrial Project EE5. http://www.gla.ac.uk/coursecatalogue/course/?code=MQSY* [Accessed: 14/12/2011]

[2] CERN, *CERN – history highlights. http://public.web.cern.ch/public/en/About/History-en.html* [Accessed: 14/12/2011]

[3] CERN, *CERN – global endeavour. http://user.web.cern.ch/public/en/About/Global-en.html* [Accessed: 14/12/2011]

[4] CERN, *CERN – The Large Hadron Collider. http://press.web.cern.ch/public/en/LHC/LHC-en.html* [Accessed: 15/12/2011]

[5] CERN, *CERN – The Missing Higgs. http://press.web.cern.ch/public/en/Science/Higgs-en.html* [Accessed: 15/12/2011]

[6] CERN, *CERN – How the LHC Works. http://press.web.cern.ch/public/en/LHC/HowLHC-en.html* [Accessed: 15/12/2011]

[7] CERN, *The introduction to the Inner Triplet System. http://www-td.fnal.gov/LHC/Uslhc_accel_docs/MQXB/Report/Intro.pdf* [Accessed: 15/12/2011]

[8] American Magnets, *Characteristics of Superconducting Magnets. http://www. americanmagnetics.com/charactr.php* [Accessed: 15/12/2011]

[9] Superconductors, *Superconductivity Explained.* http://www.superconductors.org/oxtheory.htm [Accessed: 15/12/2011]

[10] American Magnets, *Magnet Phenomena. http://www.americanmagnetics.com/magnetp.php* [Accessed: 15/12/2011]

[11] CERN, *Interim Summary Report on the Analysis of the 19 September 2008 incident at the LHC https://edms.cern.ch/file/973073/1/Report_on_080919_incident_at_LHC__2_.pdf* [Accessed: 15/12/2011]

[12] LHC-CM, *CERN - https://espace.cern.ch/LHC-CM/Circuits/Forms/AllItems.aspx* [Accessed: 11/01/2011]

[13] Fermilab, *Inner Triplet Quadrupole MQXA. http://tdserver1.fnal.gov/project/USLHC/ Specifications/LHC-MQXA-ES-0003-00-10.pdf* [Accessed: 15/12/2011]

[14] Fermilab, *Inner Triplet Quadrupole MQXB. http://tdserver1.fnal.gov/project/USLHC/ Specifications/LHC-LQX-ES-0003-10-20.pdf* [Accessed: 15/12/2011]

[15] CERN, *CERN – The LHC Design Report. http://lhc.web.cern.ch/lhc/LHC-DesignReport.html* [Accessed: 15/12/2011]

[16] CERN, *CERN – Note D'Operation Des Inner Triplets Du LHC. https://edms.cern.ch/file/1054483/1/1054483_V1_LHC-IT_Note_Operation.pdf* [Accessed: 15/12/2011]

[17] Cadence®, *Allegro AMS simulator. http://www.cadence.com/products/pcb/ams_simulator/pages/default.aspx* [Accessed: 30/12/2011]

[18] CERN, *CERN - List of Inner Triplet System Commissioning Tests. https://espace.cern.ch/LHC-CM/Circuits/RQX%20(IT)/ LHC-MPP-HCP-0011-00-30.pdf* [Accessed: 31/12/2011]

[19] CERN, *CERN – PSpice Electro-Thermal Model. https://espace.cern.ch/LHC-CM/Circuits/Forms/AllItems.aspx?RootFolder=%2FLHC%2DCM%2FCircuits%2FIPQ%2FRQ4%2FPresentations* [Accessed: 31/12/2011]

[20] CERN, *CERN - Residual Resistivity Ratio (RRR) Measurements of LHC Superconducting NbTi Cable Strands. http://cdsweb.cern.ch/record/970393/files/lhc-project-report-896.pdf* [Accessed: 03/01/2012]

[21] KAPTON®, *DuPoint™ KAPTON® - HN Polymide Film. http://www2.dupont.com/Kapton/en_US/assets/downloads/pdf/Gen_Specs.pdf* [Accessed: 11/01/2012]

Figure references

[fig 1] CERN, *CERN - http://www.cern.ch* [Accessed: 14/12/2011]

[fig 2] CERN, *CERN - List of Inner Triplet System Commissioning Tests. https://espace.cern.ch/LHC-CM/Circuits/RQX%20(IT)/ LHC-MPP-HCP-0011-00-30.pdf* [Accessed: 31/12/2011]

[fig 3] Fermilab, *Inner Triplet Quadrupole MQXA. http://tdserver1.fnal.gov/project/USLHC/ Specifications/LHC-MQXA-ES-0003-00-10.pdf* [Accessed: 15/12/2011]

[fig 4] Fermilab, *Inner Triplet Quadrupole MQXB. http://tdserver1.fnal.gov/project/USLHC/ Specifications/LHC-LQX-ES-0003-10-20.pdf* [Accessed: 15/12/2011]

[fig 5] CERN, *CERN – PSpice Electro-Thermal Model. https://espace.cern.ch/LHC-CM/Circuits/Forms/AllItems.aspx?RootFolder=%2FLHC%2DCM%2FCircuits%2FIPQ%2FRQ4%2FPresentations* [Accessed: 31/12/2011]

DATASHEETS

[ds1] International Rectifier – *D245NQ015N(R) Schottky Rectifier Diode, 240A*

[ds2] EUPEC – *TZ425N Phase Control Thyristor Module, 800A*

[ds3] EUPEC – *T3709N02..04 Phase Control Thyristor, 7kA*

[ds4] EUPEC – *D4457N Power Rectifier Diode, 7kA*

List of Equations

Equation 1: $\boldsymbol{R_{cable} = \rho_{cable}\left(\frac{L_{cable}}{A_{cable}}\right)}$

R_{cable} - *resistance of the cable,* ρ_{cable} - *resistivity of the cable,* L_{coil} - *length of the cable,* A_{cable} - *Cross-sectional area of the cable*

Equation 2: $\boldsymbol{Q(t) = 1 - exp\left(-\left(\frac{t}{\tau}\right)^{\gamma}\right)}$

$Q(t)$ - *Quench factor, t - time,* τ - *estimated time to quench variable,* γ - *variable effects estimation of the rate of change of quench propagation velocity*

Equation 3: $\boldsymbol{V(t) = I(t)R(t)}$

$V(t)$ - *voltage,* $I(t)$ - *current,* $R(t)$- *resistance*

Equation 4: $\boldsymbol{I(t) = \int_0^{\infty} \frac{\Delta V_{mag}}{L_{mag}} dt}$

$I(t)$ - *current,* ΔV_{mag} - *difference in voltage across magnet,* L_{mag}- *inductance of the magnet*

Equation 5: $\boldsymbol{\Delta V(t) = \int_0^{\infty} \frac{I_{mag}}{C_{mag}} dt}$

$\Delta V(t)$- *difference in voltage,* I_{mag}- *current in the magnet,* C_{mag}- *capacitance of the magnet*

Equation 6: $\boldsymbol{RRR_{mag} = \frac{\rho_{293K}}{\rho_{1.9K}}}$

RRR_{mag}- *Residual Resistivity Ratio of the magnet,* ρ_{293K} - *resistivity at warm,* $\rho_{1.9K}$ - *resistivity at cold*

Equation 7: $\boldsymbol{\rho_{Cu,thermal} = 0.37 + \left(\frac{1.7}{RRR_{mag}} + \frac{1}{\left(\frac{2.33G}{\Delta T_{cable}{}^5}\right)+\left(\frac{957k}{\Delta T_{cable}{}^3}\right)+\left(\frac{163}{\Delta T_{cable}}\right)}\right)n + \left(\frac{500\mu}{RRR_{mag}} \times B_{mag}\right)0.1n}$

$\rho_{Cu,thermal}$ - *thermal resistivity of copper,* RRR_{mag} - *Residual Resistivity Ratio of the magnet,* ΔT_{cable} - *change in temperature of the cable,* B_{mag}- *magnets' magnetic field strength*

Equation 8: $\boldsymbol{\frac{1}{R_{tot}} = \frac{1}{R_{Cu}} + \frac{1}{R_{NbTi}}}$

R_{tot} - *total resistance,* R_{Cu} - *resistance of copper,* R_{NbTi} - *resistance of niobium-titanium*

Equation 9: $\boldsymbol{R_{tot,electrical}(t) = \left((\rho_{Cu,NSC} + \rho_{Cu,SC})Q(t)\right) + \left((\rho_{NbTi,NSC} + \rho_{NbTi,SC})Q(t)\right)}$

$R_{tot,electrical}(t)$ - *total electrical resistance,* $\rho_{Cu,NSC}$ - *resistivity of copper, non-superconduting state,* $\rho_{Cu,SC}$ - *resistivity of copper, superconducting state,* $Q(t)$- *Quench factor function*

Equation 10: $\boldsymbol{\sigma_{Cu,thermal} = \frac{\Delta T_{cable}}{\rho_{Cu,thermal}} \times 24.5n}$

$\sigma_{Cu,thermal}$ - *thermal conductivity of copper,* ΔT_{cable} - *difference in temperature of cable,* $\rho_{Cu,thermal}$ - *thermal resistivity of copper*

Equation 11: $\boldsymbol{R_{thermal} = \frac{1}{\sigma_{Cu,thermal}} \times W_{mag}}$

$R_{thermal}$ - *thermal resistance,* $\sigma_{Cu,thermal}$ - *thermal conductivity of copper,* W_{mag} - *width of magnet*

Equation 12: $\boldsymbol{C_{thermal} = \left(\left(\frac{\frac{Cu}{NbTi}}{\frac{Cu}{NbTi}+1}\right) Q_{Cu} + \left(\frac{Cu}{NbTi}\right) Q_{NbTi}\right) \times \frac{\pi D_{cable}{}^2}{4 N_s L_{cable}}}$

$C_{thermal}$ - *thermal capacitance,* Q - *thermal capacity,* D_{cable}- *cable diameter,* N_s - *number of strands,* L_{cable}, *length of cable*

Equation 13: $\boldsymbol{\Delta T_{cable}(t) = T_{cable}(t) - T_{cable,1.9K} = \frac{\left(P_{thermal}(t) - \frac{d}{dt}(C_{thermal} \times \Delta T_{cable}(t))\right)}{R_{thermal,cable} + R_{thermal,ins}}}$

ΔT_{cable} - *difference in temperature of cable,* $P_{thermal}$- *thermal power,* $C_{thermal}$ - *thermal capacitance,* $R_{thermal,cable}$, - *thermal resistance of cable,* $R_{thermal,ins}$, - *thermal resistance of insulation layer*

Equation 14: $\boldsymbol{P_{thermal}(t) = I_{coil}(t) \times R_{tot,electrical}(t)}$

$P_{thermal}$- *thermal power,* I_{coil}- *current in magnet coil,* $R_{tot,electrical}(t)$ - *total electrical resistance*

Equation 15: $\boldsymbol{B_{mag}(t) = I_{mag}(t) \times TF_{mag}}$

B_{mag}- *magnets' magnetic field strength,* I_{mag}- *current in magnet,* TF_{mag}, - *magnet transfer function*

Equation 16: $\boldsymbol{E_{stored} = \frac{1}{2} L_{mag} I_{mag}}$

E_{stored}, *energy stored,* L_{mag}- *inductance of the magnet,* I_{mag}- *current in magnet*

Equation 17: $\boldsymbol{E_{dissipated}(t) = \int_{t_{quench}}^{\infty} I_{mag} \Delta V_{mag} dt}$

$E_{dissipated}$, *energy dissipated,* t_{quench}- *time of quench initiation,* I_{mag}- *current in magnet,* ΔV_{mag} - *difference in voltage across magnet*

Equation 18: $\boldsymbol{\int_{t_{quench}}^{\infty} I_{mag}{}^2 = 10^6 MIITs - \int_0^{t_{quench}} I_{mag}{}^2}$

MIITs - *superconducting magnet quench parameter,* t_{quench}- *time of quench initiation,* I_{mag}- *current in magnet,*

Equation 19: $\boldsymbol{R_{eff,min} = \frac{I_{mag}{}^2 L_{mag}}{10^6 MIITs - \int_0^{t_{quench}} I_{mag}{}^2}}$

$R_{eff,min}$, *minimum safe resistance,* MIITs - *superconducting magnet quench parameter,* t_{quench}- *time of quench initiation,* I_{mag}- *current in magnet,*

APPENDICES*

*Following appendices are not exhaustive. Large files/code/presentations are on a provided Compact Disk (CD)

Appendix A - Basic Circuit Model User Guide

Appendix A.1 Opening Model

- Load Cadence® Suite Project Manager.
- Load Project Named RQX.
- Open Design.

Appendix A.2 Changing Circuit/Circuit Type

- To simulate an event from a different circuit, change the values of the busbar resistance, e.g. RRQXBUSQ1, as according to the Electrical Circuits Layout Database.
- To change the circuit type, cut the components in parallel with Q1 and Q3 magnets and paste them in parallel with the opposite magnets.

Appendix A.3 Changing Circuit Simulation Test

- Each PC current source has an implementation name. Alter this implementation name to the desired test title, e.g. RQX_PNO.D16.
- Also change the implementation of the voltage sources that trigger the thyristors to the corresponding simulation test.

Appendix A.4 Using AMS Simulator

- Once the test is set-up, open the simulation editor and set your desired values.
- Click run on the DEHDL command window. AMS should 'bridge' with DEHDL and begin running the simulation.
- Upon completion of the simulation, go to 'File – Run Commands' and run the command files 'ALL'. Note: if you wish to see a specific plot in AMS, use the 'Add Trace' option to manually plot any desired graph.

Appendix A.5 Convergence Errors/Solutions

As it stands, the circuit model is still subject to convergence errors upon changing simulations. To get around this problem, try some of the following:

- Check that no errors in altered values have been made.
- Alter the time step in the simulation editor; both smaller and larger time steps may work.
- Alter the BREAKSTEP ABM components, to manually dictate different time steps at specific times throughout the simulation.
- Add/Remove parasitic resistances/capacitances around the most troublesome components to smooth out the simulation.

Appendix B - Extracting and Analysing/Comparing Data

Appendix B.1 Used Procedure for the Comparison of Data

Confirming the accuracy of the final model required an in depth comparison of simulation data with recorded LHC's PM data, across a wide range of tests. The procedure carried out required the acquisition of both simulation and LHC's PM data in a simple numerical text file. To achieve this, the use of CERN's PM events database was required, as it is able to access any recorded event since the LHC's construction. This database was used to extract recorded LHC's PM data as a comma separated value (**.csv**) file. With regard to the simulation data, the AMS simulator gives the option of extracting plotted data in a wide range of file formats. Choosing .csv files made generating comparisons inherently simpler.

Appendix B.2 MathWorks® MATLAB® Data Comparison Script

As mentioned in **section 3.3,** for direct comparison and plotting of the acquired data files, MATLAB® was used. Due to the great amount of comparisons and subsequent simulations/event analysis it was advised that a script be written to produce all comparative/desired simulation plots. Brief descriptions of the structures and functions follow. A full copy of an example script file can be found in the corresponding file of the submitted CD.

Read LHC Data.csv

Firstly, the code utilises the csvread( ) function to import data extracted from the PM browser. This is done separately for both currents and voltages.

Clean LHC Data.csv

Following that, a cleaning script utilised the isnan( ) function to remove NaN values generated by the PM measurements allowing for accurate matching of data to a given time stamp.

Read AMS Data.csv

Secondly, the code reuses the csvread( ) to import the data extracted from the AMS. Again, this is done separately for both currents and voltages.

Plot ALL function

The script then uses the plot( ) function to automatically generate all the desired graphs, with specific colouring and labelling, saving each generated figure in both .fig and .jpg formats.

Appendix C - Tables

Appendix C.1 Tables of AMS Model Editor Parameters for Circuit Components

The following is the list of tables of the final component parameters as generated when using the AMS Model Editor.

Appendix C.1.1 Table of Model Editor Parameters for D245NQ015R Diode

Table 7: List of parameters generated by AMS Model Editor for the D245NQ015R Diode

Parameters	Abb	Values	
Saturation Current	IS	1.93186E-02	A
Emission Coefficient	N	1.15684E+00	
Resistance	RS	2.37362E-04	Ω
High-Inject Knee Current	IKF	2.60259E+02	A
Saturation Current Temp coeff	XTI	3.00000E+00	
Energy of Bandgap	EG	1.11000E+00	eV
Junction Capacitance	CJO	2.85375E-09	F
Grading Coefficient	M	3.02598E-01	
Junction Potential	VJ	3.90500E-01	V
Depletion Capacitance coeff	FC	5.00000E-01	
Recombination Current	ISR	5.38782E-02	A
Emission Coefficient of ISR	NR	4.99500E+00	
Reverse Breakdown Voltage	BV	1.50000E+01	V
Reverse Breakdown Current	IBV	4.00000E-02	A
Carrier Transit Time	TT	5.00000E-09	s

Appendix C.1.2 Table of Model Editor Parameters for D4457N Diode

Table 8: List of parameters generated by AMS Model Editor for the D4457N Diode

Parameters	Abb	Values	
Saturation Current	IS	4.21700E-03	A
Emission Coefficient	N	2.59000E+00	
Resistance	RS	1.71970E-05	Ω
High-Inject Knee Current	IKF	1.00000E+03	A
Saturation Current Temp coeff	XTI	3.00000E+00	
Energy of Bandgap	EG	1.11000E+00	eV
Junction Capacitance	CJO	1.00000E-12	F
Grading Coefficient	M	3.33300E-01	
Junction Potential	VJ	7.50000E-01	V
Depletion Capacitance coeff	FC	5.00000E-01	
Recombination Current	ISR	1.00000E-10	A
Emission Coefficient of ISR	NR	2.00000E+00	
Reverse Breakdown Voltage	BV	2.00000E+02	V
Reverse Breakdown Current	IBV	6.00000E-02	A
Carrier Transit Time	TT	1.00000E-02	s

Appendix C.1.3 Table of Model Editor Parameters for TZ425N Thyristor

Table 9: List of the parameters entered into AMS Model Editor for the TZ425N Thyristor

Parameters	Abb	Values	
Peak Forward Voltage	Vdrm	1200	V
Peak Reverse Voltage	Vrrm	1400	V
Holding Current	Ih	300	mA
On-state Voltage	Vtm	1.5	V
On-state Current	Itm	800	A
Rate of Change of Voltage	dVdt	1000	10^6
Gate Trigger Current	Igt	250	mA
Gate Trigger Voltage	Vgt	1.5	V
Gate Controlled Delay Time	Ton	4	us
Turn Off Time	Toff	250	us
Peak Forward Current	Idrm	80	mA

Appendix C.1.4 Table of Model Editor Parameters for T37902N Thyristor

Table 10: List of the parameters entered into AMS Model Editor for the T37902N Thyristor

Parameters	Abb	Values	
Peak Forward Voltage	Vdrm	400	V
Peak Reverse Voltage	Vrrm	600	V
Holding Current	Ih	300	mA
On-state Voltage	Vtm	1.5	V
On-state Current	Itm	7000	A
Rate of Change of Voltage	dVdt	1000	10^6
Gate Trigger Current	Igt	250	mA
Gate Trigger Voltage	Vgt	2	V
Gate Controlled Delay Time	Ton	13	ms
Turn Off Time	Toff	1	us
Peak Forward Current	Idrm	250	mA

Appendix C.2 Table of Cable Resistances with Corresponding Simple Schematic Drawing

Table 11: Plot of the Calculated Cable resistances in accordance to the basic schematic diagram shown below

Copper resistivity						
			Resistivity(Ωm) @20°C	1.75E-08	1.72E-08	1.68E-08
	Area (m^2)	Length(m)				
PURPLE	2.40E-04	9	Resistance(Ω)	6.56E-04	6.45E-04	6.30E-04
ORANGE	2.50E-05	9	R=((pL)/A)	6.30E-03	6.19E-03	6.05E-03
RED	3.00E-04	1.5		8.75E-05	8.60E-05	8.40E-05
GREEN	3.50E-05	1.5		7.50E-04	7.37E-04	7.20E-04
BAR	2.50E-04	2		1.40E-04	1.38E-04	1.34E-04

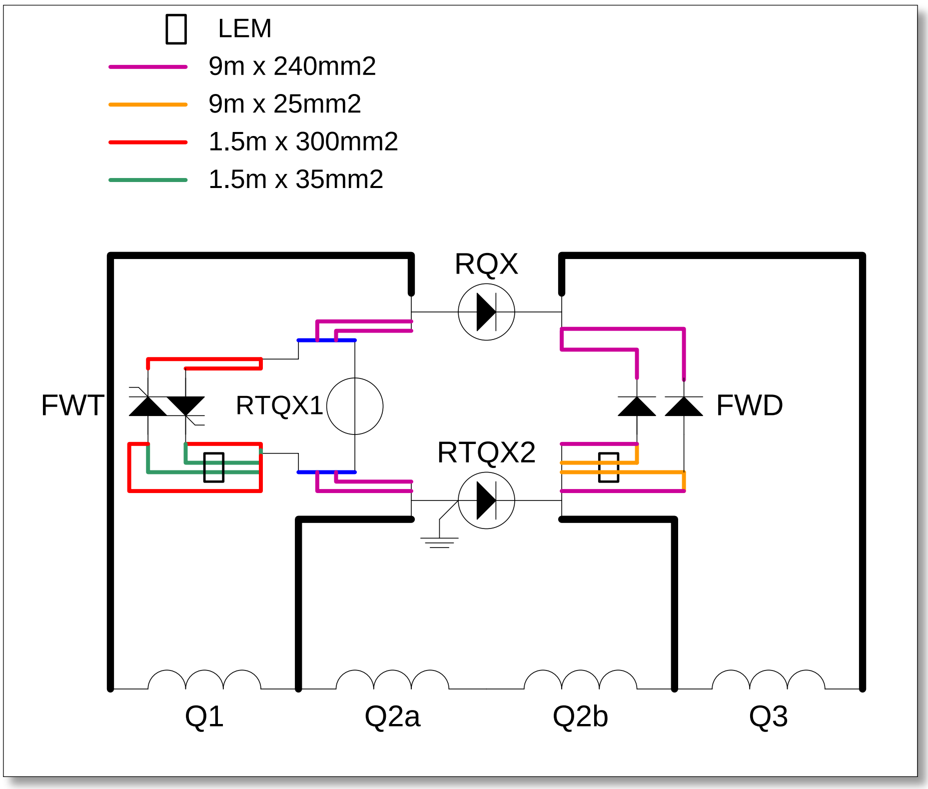

Figure 35: Schematic Diagram showing the cables in the system, coloured according to their listed dimensions

Appendix D - Further Simulation Results

Appendix D.1 Full Comparative Analysis Plots for PLI3.f6

The following plots contain an example of the full analysis as generated by the comparative simulation code. The simulation run was that of a quench in the ITS, according to the commissioning test PLI3.f6. This test had been validated with PM recorded in terms of the simulated currents and voltages.

RQX.L8, PLI3.f6 – Quench@50% Current, All 3 PCs Active, RTQX1 Positive

This simulation represents any event in which the QPS is triggered. This could have been a naturally occurring quench due to the surpassing of the critical current, magnetic field, temperature or strain thresholds. It may also have been an accidental triggering due to a threshold within the QPS being crossed, though a quench may, in fact, have occurred.

Current Flow through PCs

Shown below is a comparative plot of the currents in the PC current loops. It is clear that the simulated data and the recorded data follow the same characteristics. This level of accuracy is reason to believe that the following analytical graphs illustrate accurate values.

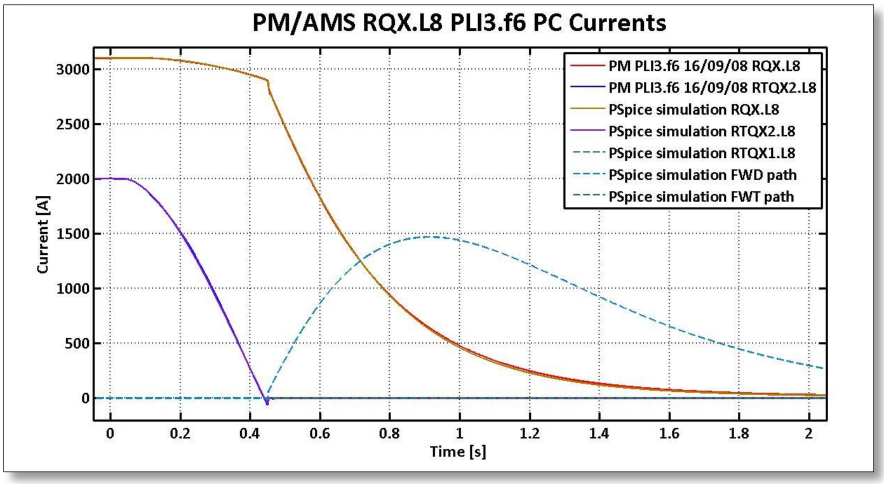

Voltage Potential across PCs

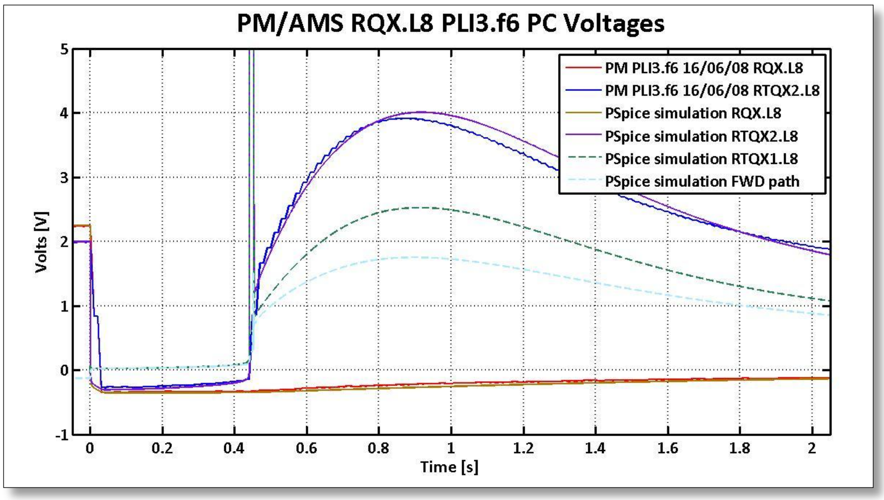

Current Flow through PC Diodes/FWT/FWD paths

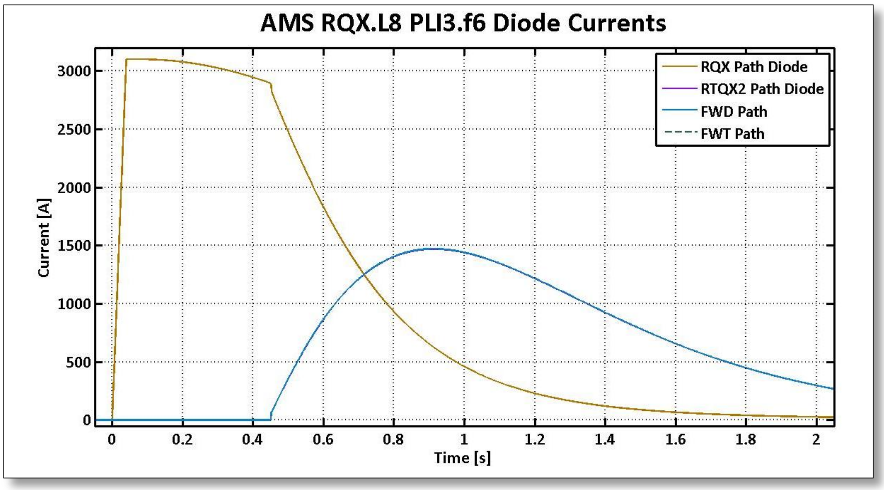

Current Flow through Busbars

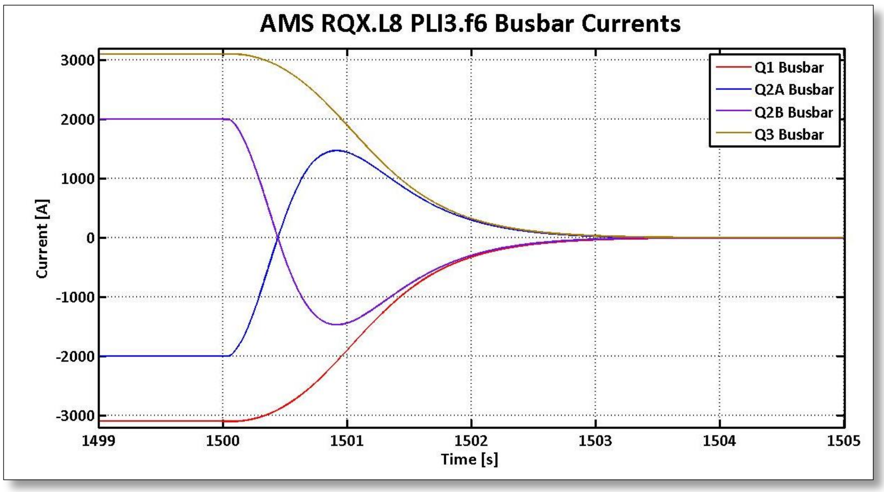

Voltage Potential across Busbars

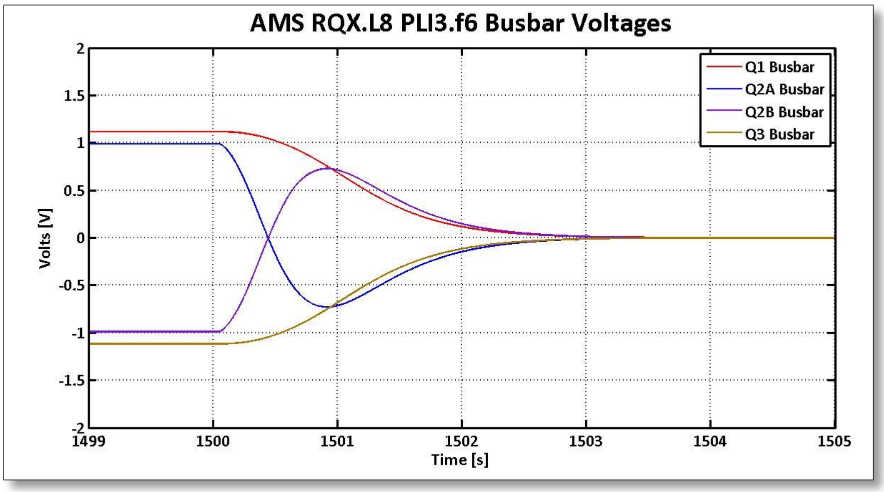

Current Flow through Magnets

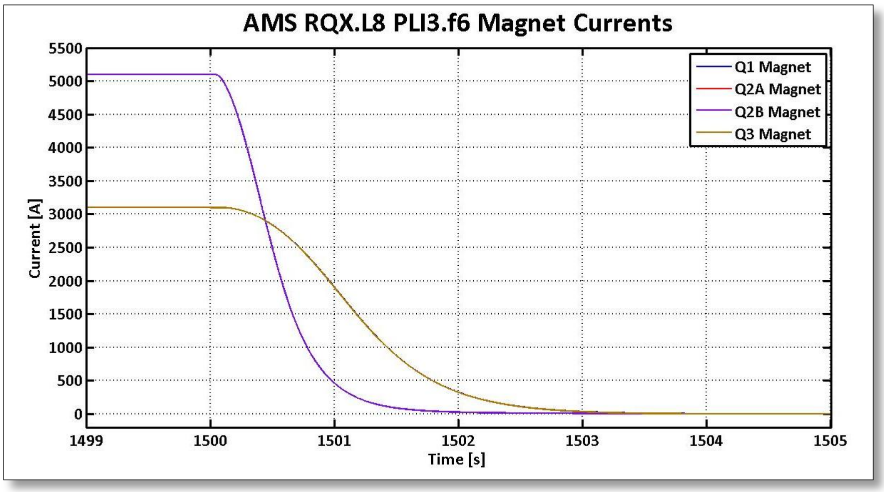

Magnetic Field Strength

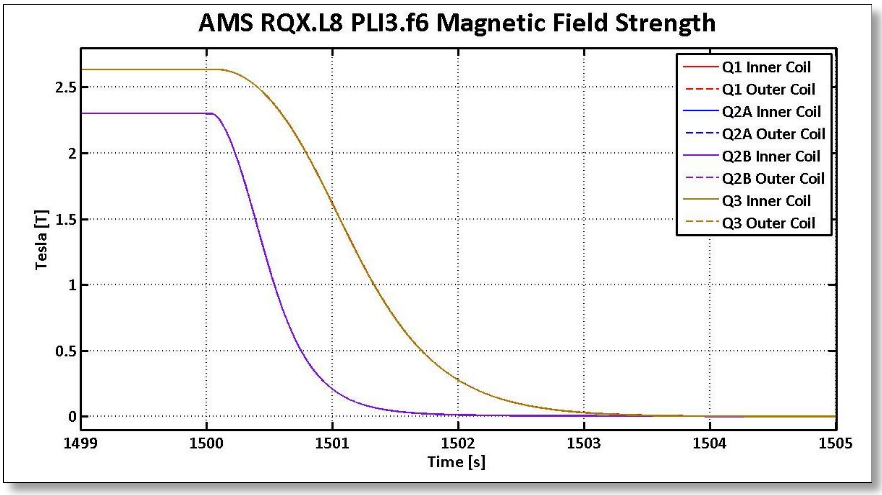

Energy Stored in Magnets

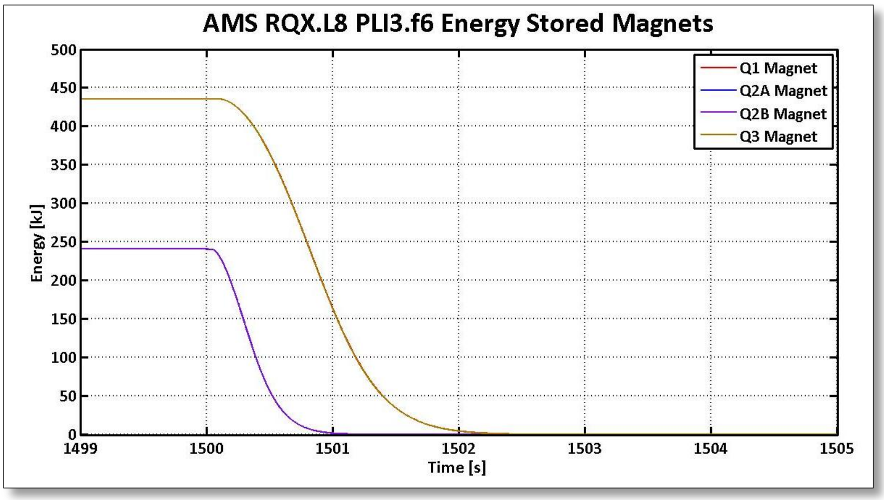

Energy Dissipated in Magnets

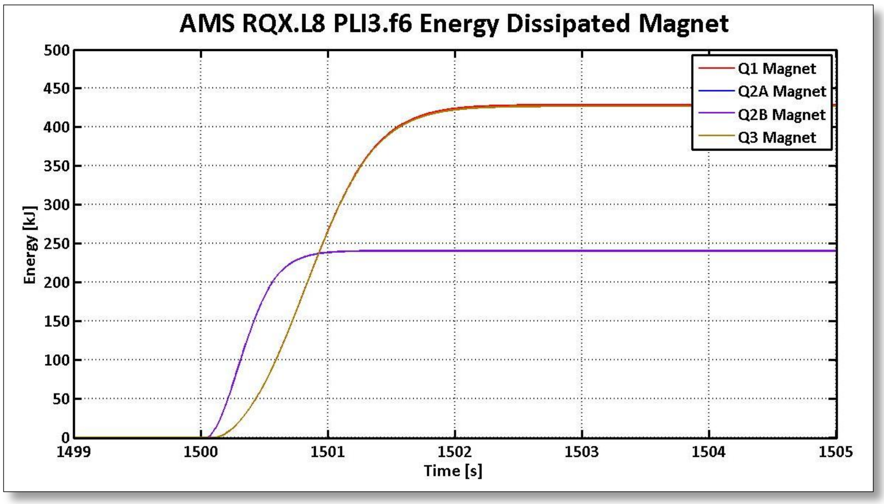

Energy Dissipated in PC Diodes

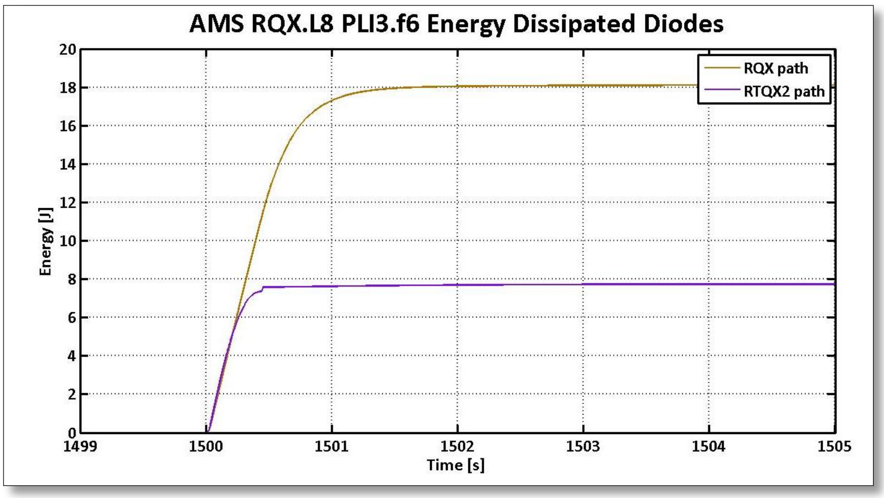

Electrical Resistance of Magnet Coils

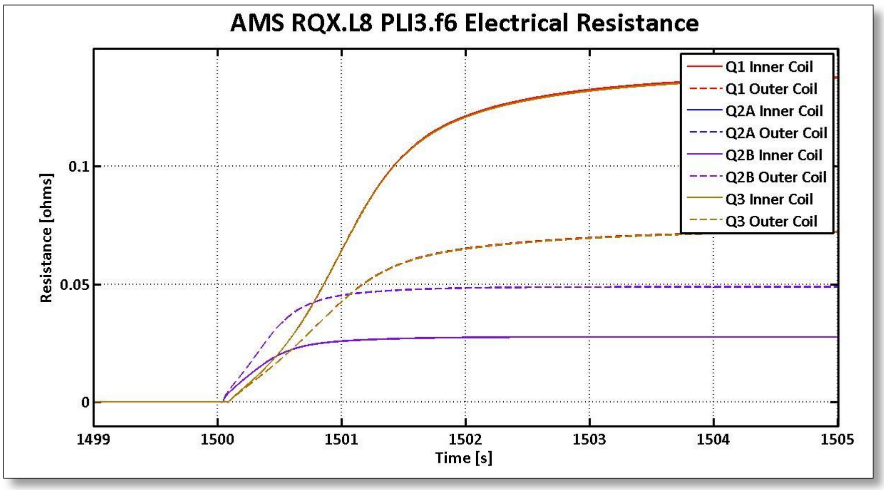

Temperature of Magnet Coils

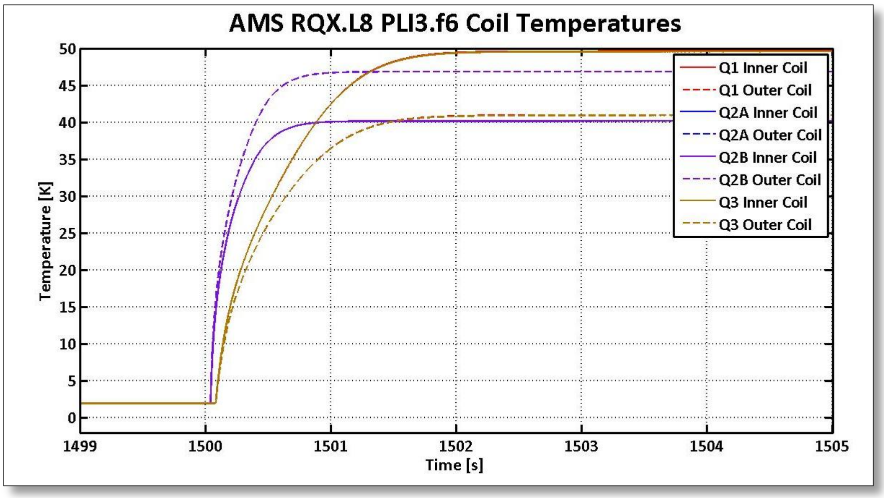

Thermal Capacity of Magnet Coils

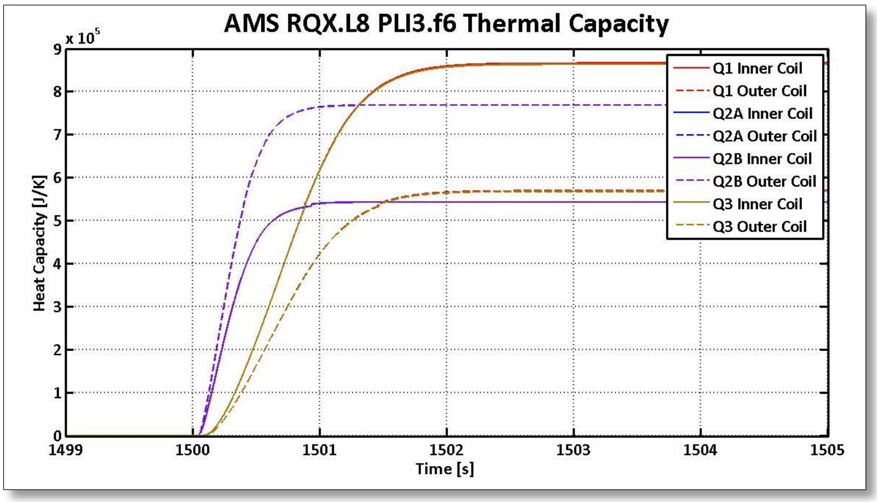

Thermal Power of Magnet Coils

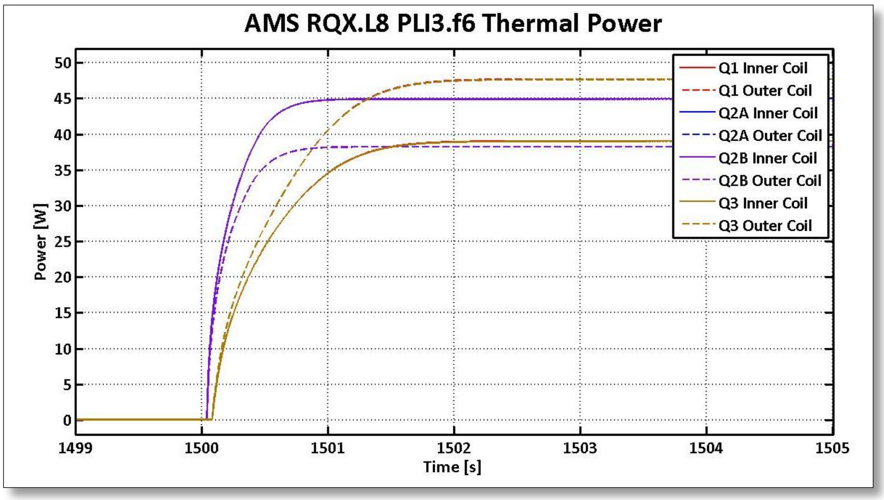

MIITs of Magnets

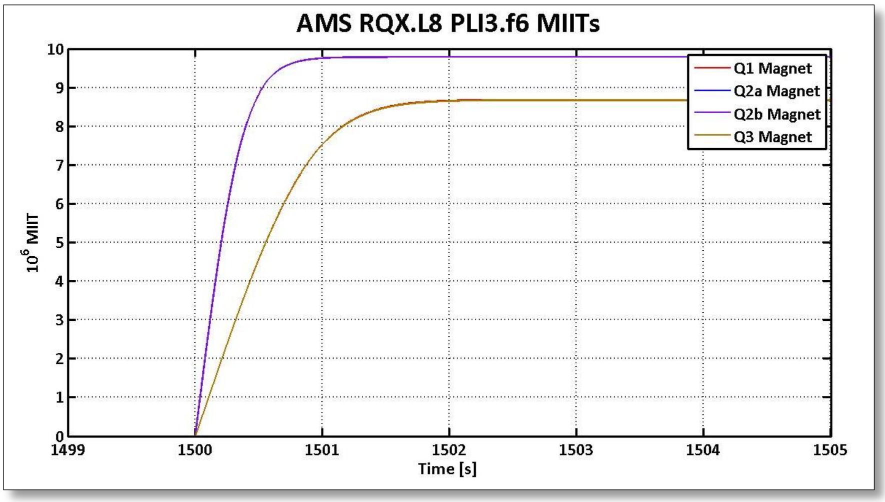

Quench Factor

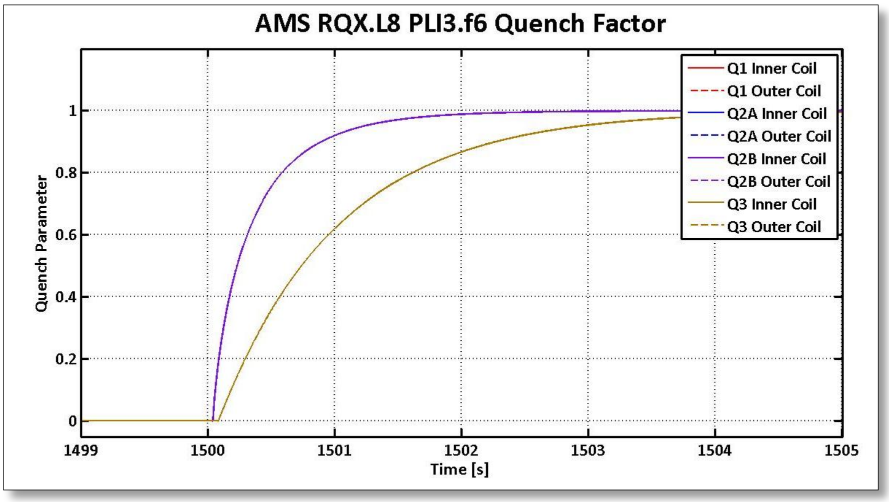

Appendix E - Design Schematics

Appendix E.1 Simple schematic

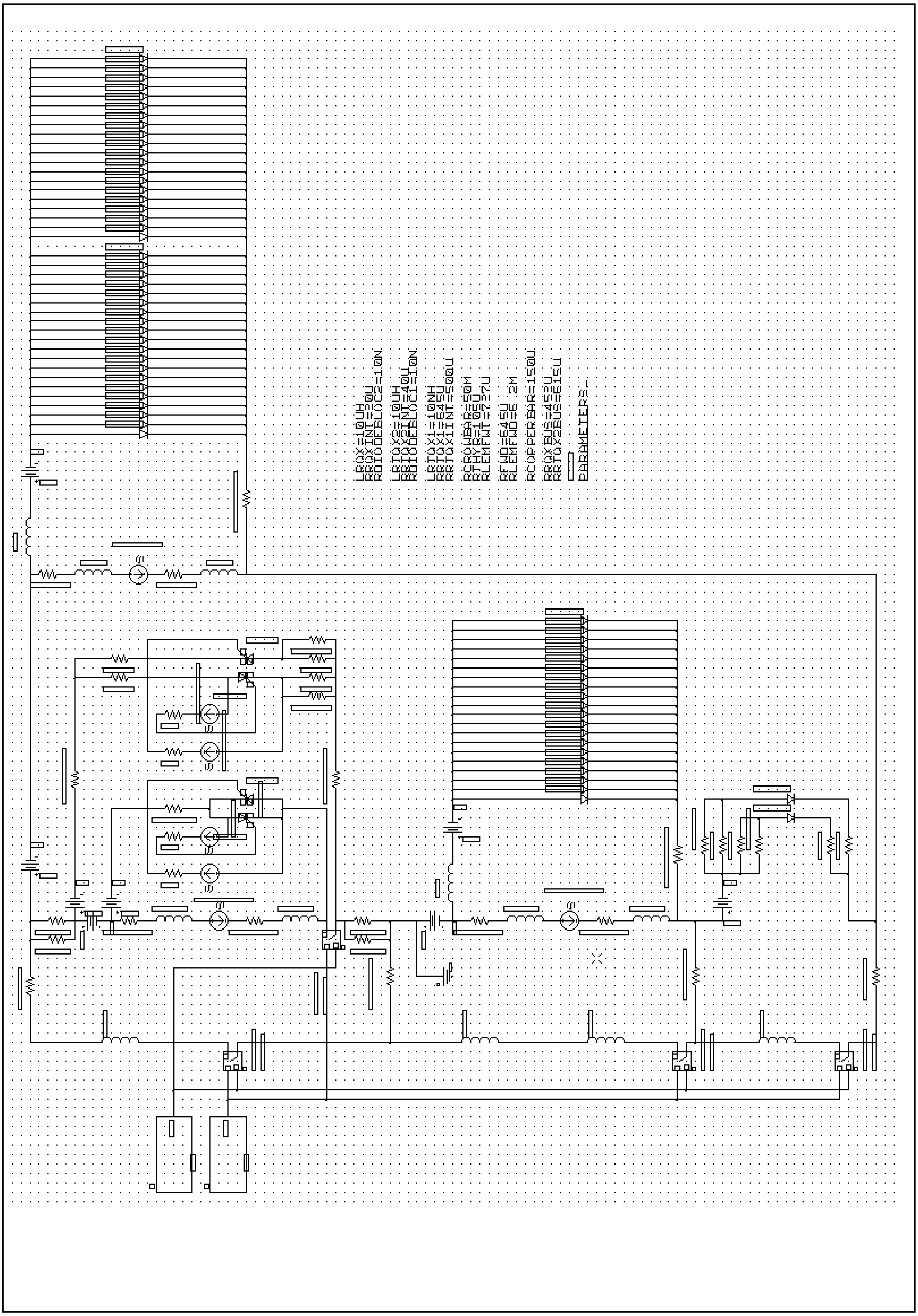

Appendix E.2 Thyristor triggering Type 1

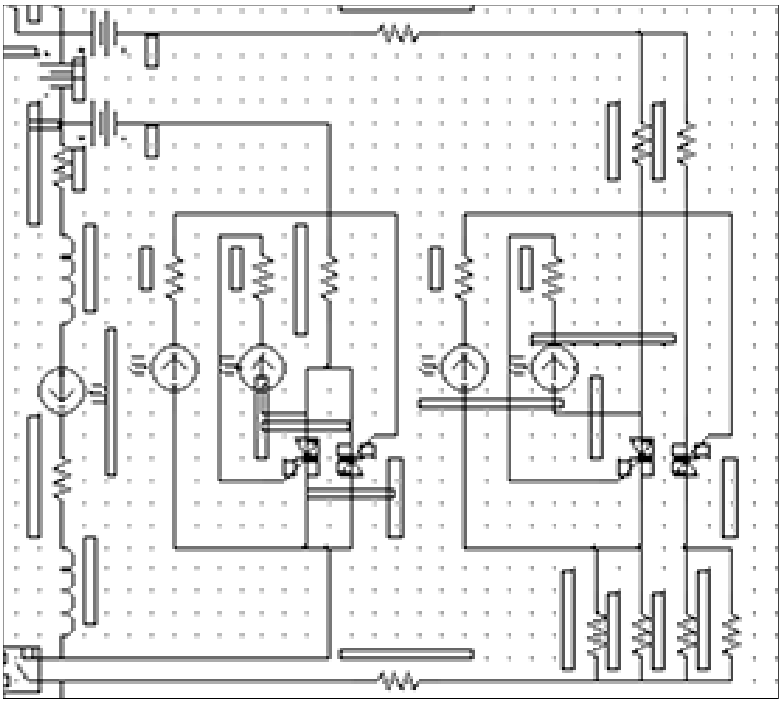

Appendix E.3 Thyristor triggering Type 2

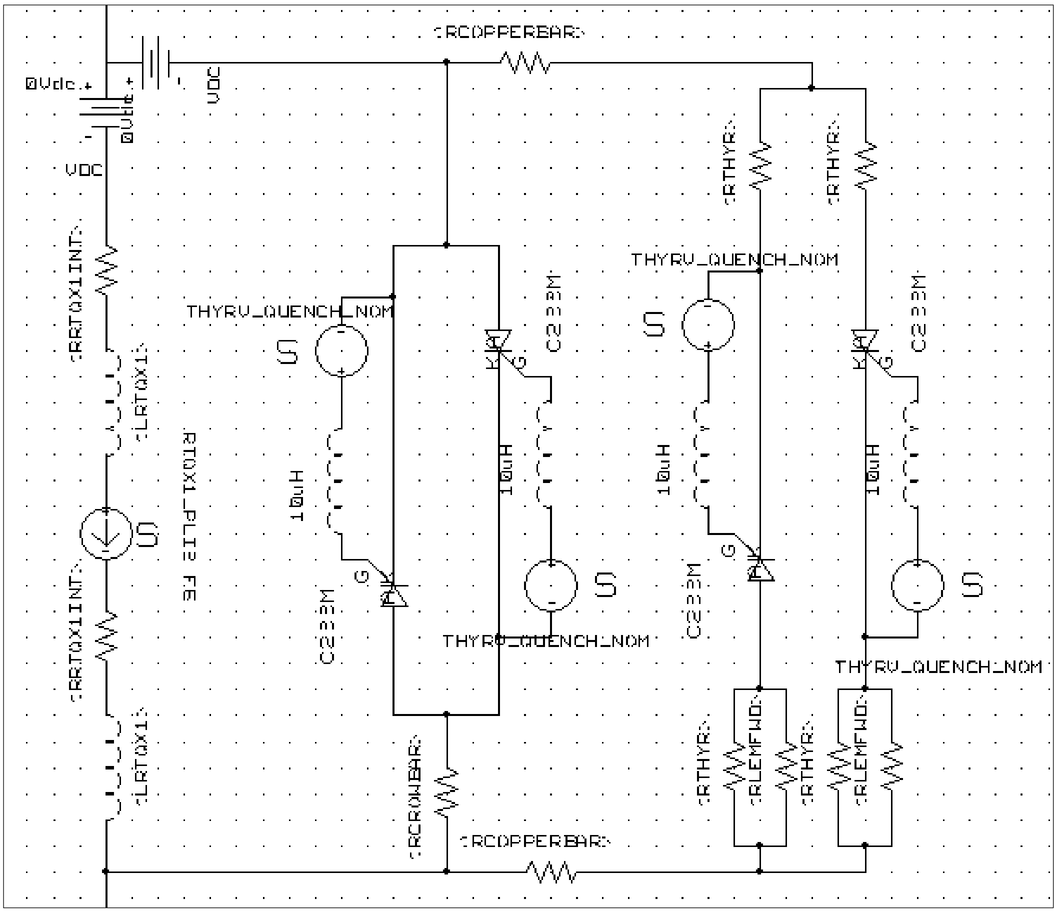

Appendix E.4 Schematic of Cable Temperature Section of the Electro-Thermal Model

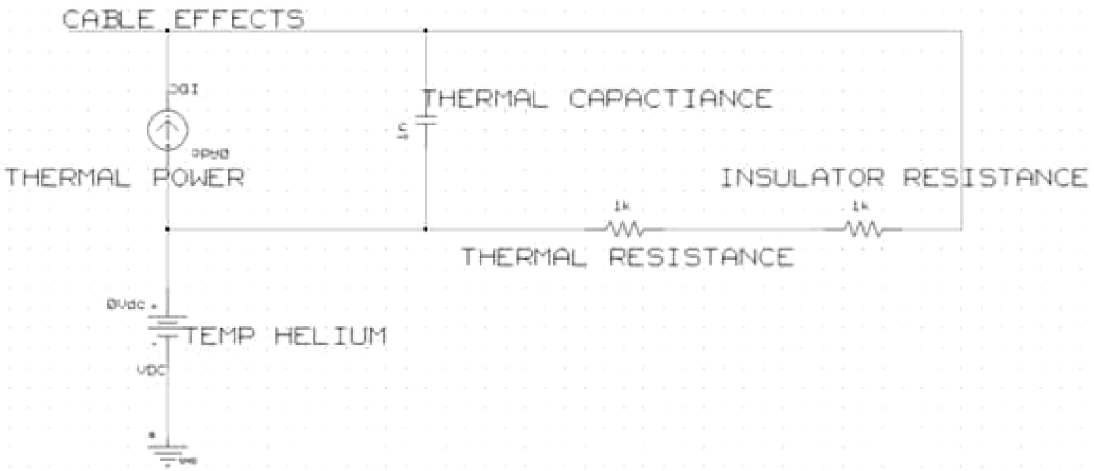

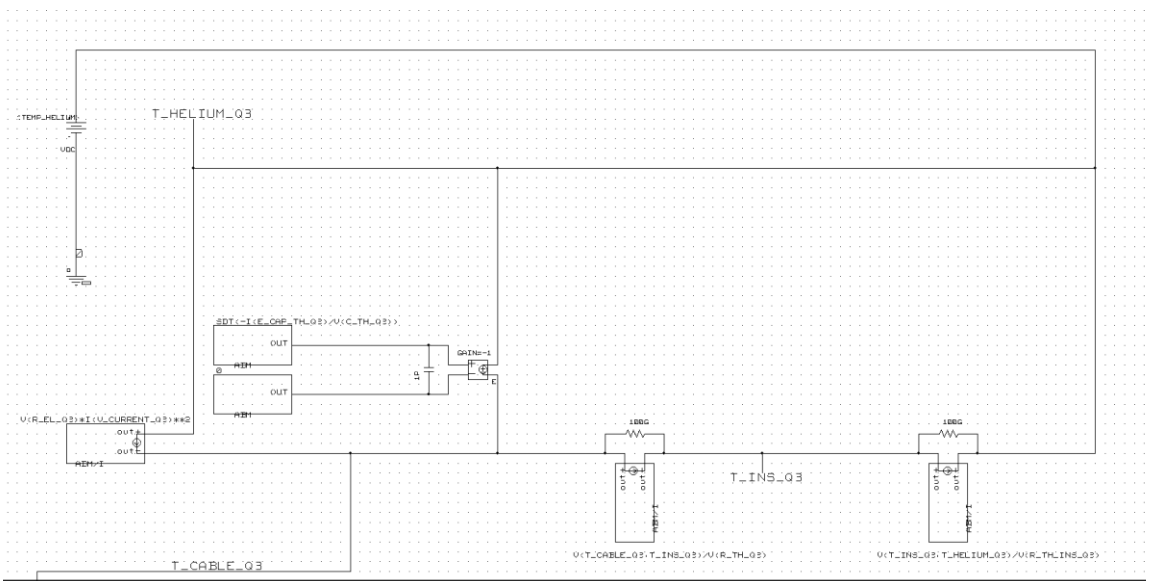

Appendix E.5 Schematic of Electro-Thermal Model

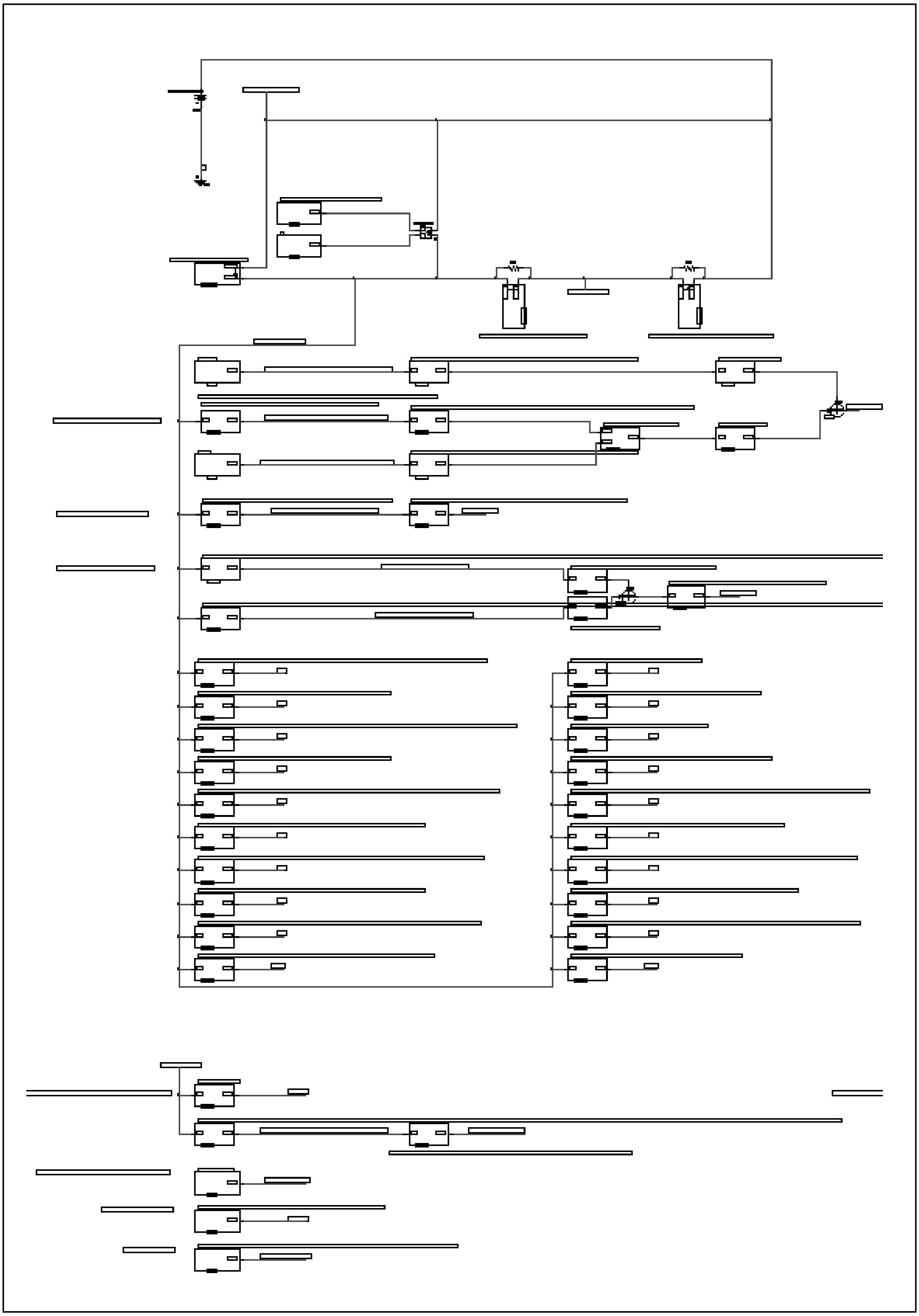

Appendix E.6 Schematic of Circuit Model with Electro-Thermal Model for Each Magnet

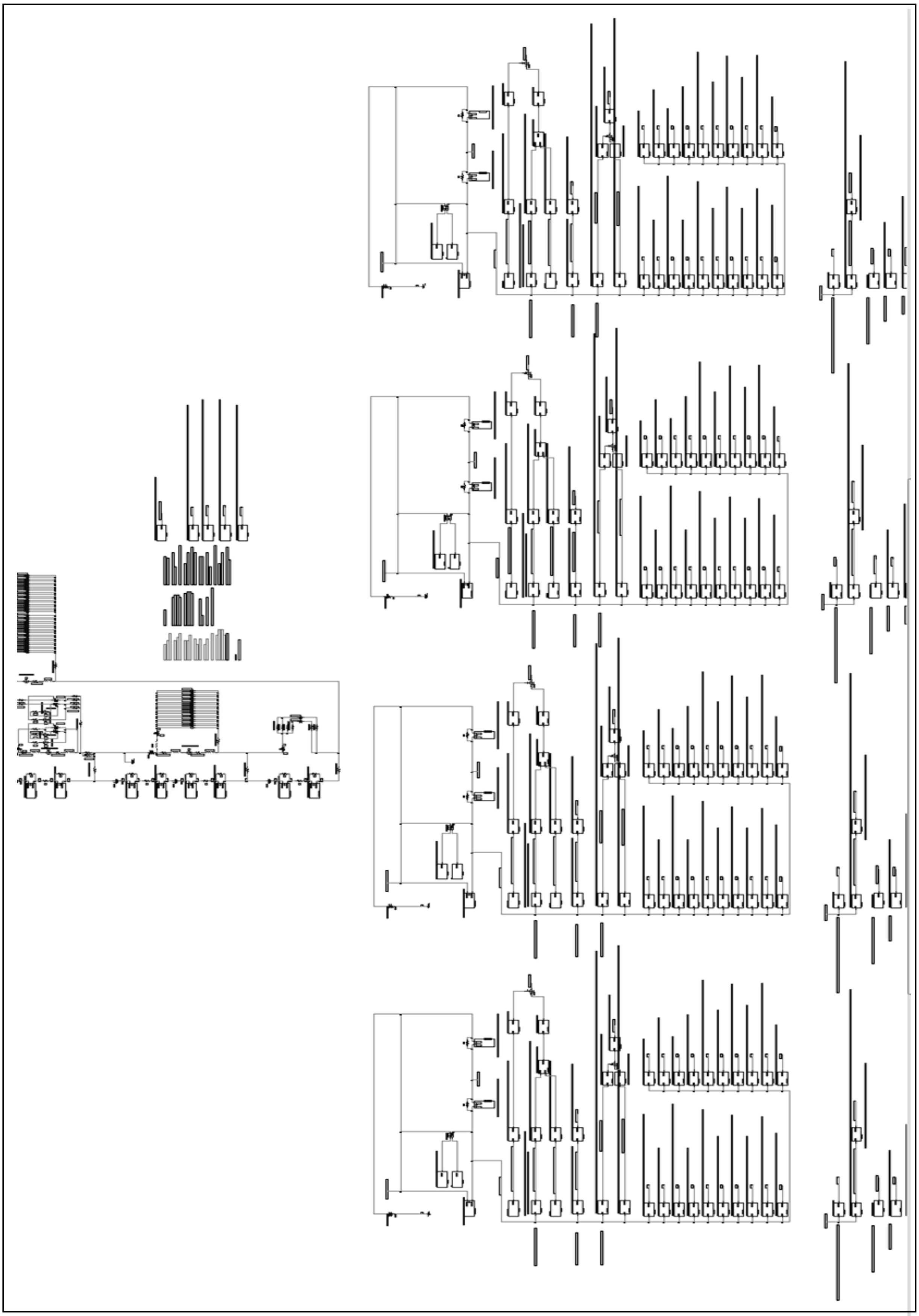

Appendix E.7 Final Schematic of Circuit Model with Separate Electro-Thermal Model for Each Magnet Coil

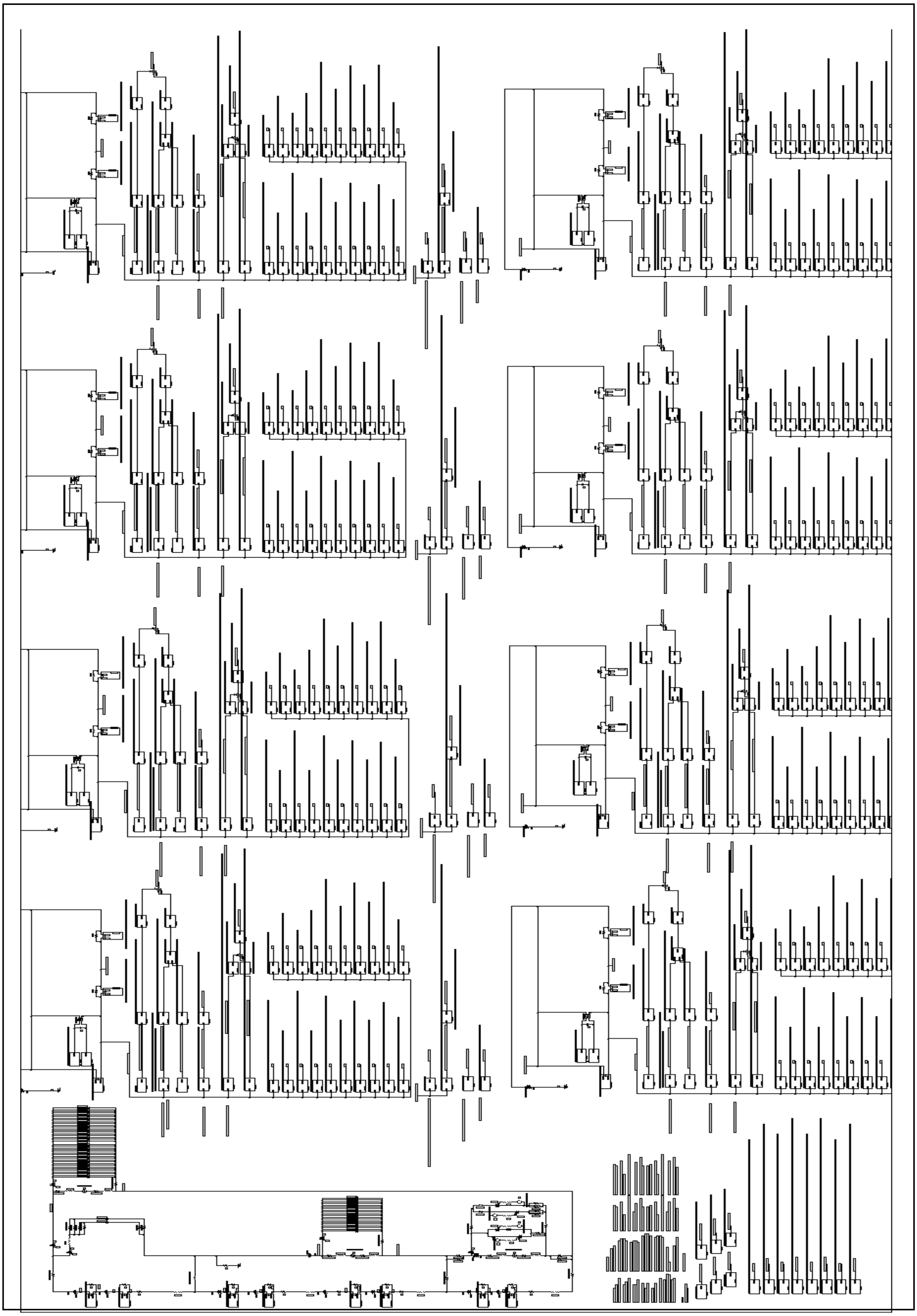

Appendix E.8 Schematic of Final Parameter List

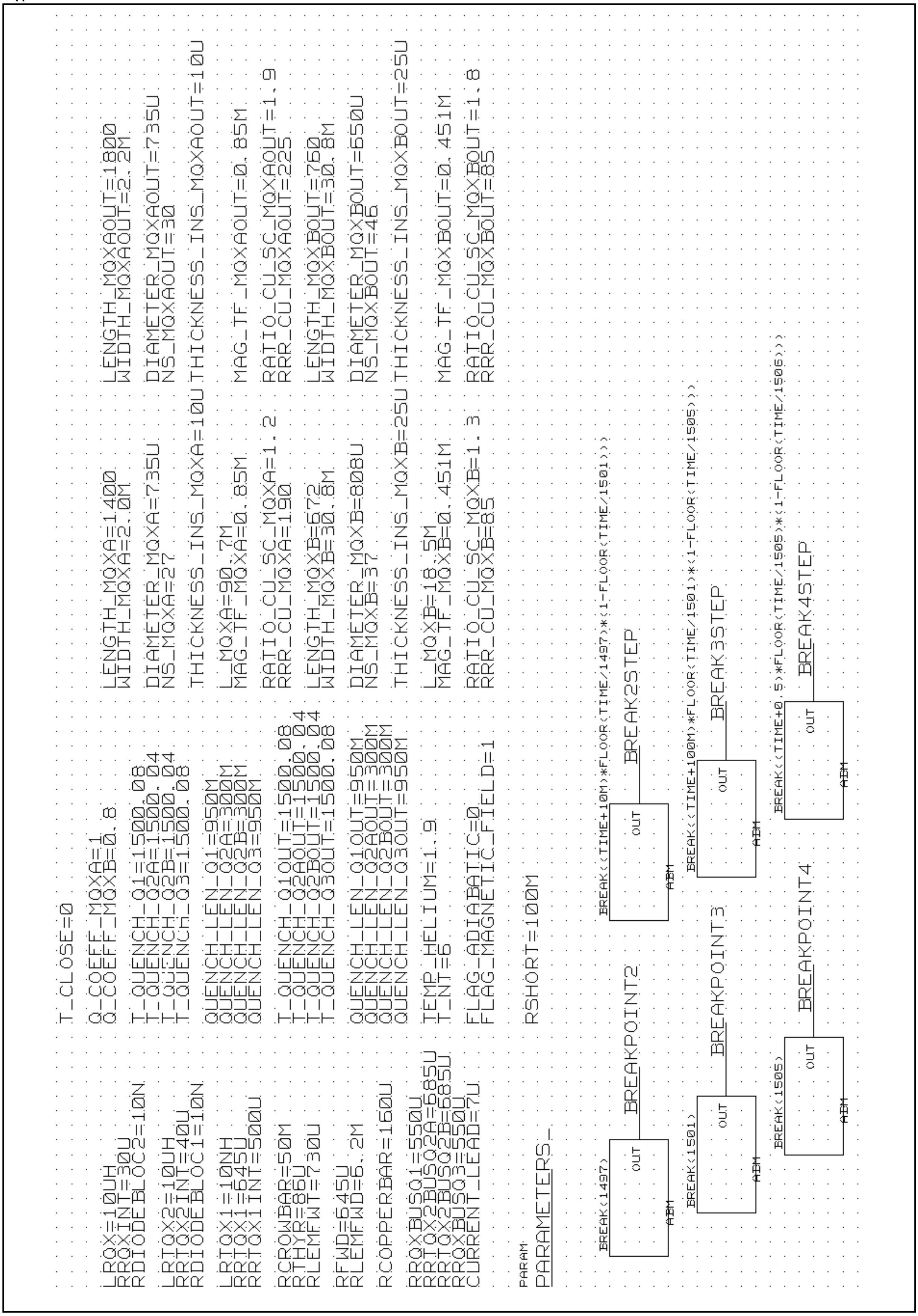

Appendix F - Simulation Code and Data Comparison Scripts

Throughout the duration of the project, several scripts for the simulation of a specific test and for the plotting of desired data had to be programmed. The following, is a list of the written scripts, which can be found in the corresponding files of the submitted CD.

Appendix F.1 Code for Current and Voltage Source Stimulus

For the current and voltage sources present in the circuit model, source stimulus had to be manually entered according to the defined commission tests.

Appendix F.2 Code for AMS to Generate All Useful Plots for Analysis

To make plotting of the analysis of a simulation less time-consuming, a command file was written to be used within AMS simulator to generate all the desired plots by simply using the 'Run commands' option.

Appendix G - Slides of Presentations

Throughout the course of my placement, I was asked to make, and gives regular presentations. The following appendices list the titles of the presentations and their section headings. For the full presentation slides, as created in Microsoft® PowerPoint®, please see the corresponding files in the submitted CD.

Appendix G.1 - LHC-CM 2011-06-24 by Scott Rowan

Introduction to system
Device modelling
Design Entry HDL Schematics
AMS simulations

Appendix G.2 - LHC-CM 2011-08-04 by Scott Rowan

Recap
Updates
AMS/PM comparison
Unexplained anomalies
Further work

Appendix G.3 - LHC-CM 2011-07-09 by Scott Rowan

Recap
Thermal model of magnets
RQX circuit event list
Quench analysis/simulations
Interesting anomalies
Further work

Appendix G.4 - LHC-CM 2011-10-24 by Scott Rowan

Recap
Circuit Model Updates
Quench PM Comparison
Full Current Quench Simulations
Failure Simulations
Further work

Appendix G.5 - TE-MPE-PE 2011-11-02 by Scott Rowan

(This presentation, presented to the whole section, was to be a concise review of the obtained results)
Circuit Analysis/Current Flow during FPA/Quench
PSpice/PM data Comparison during FPA/Quench
List of Useful Information Available from Simulations

Appendix H - Industrial Project EE5 Interim Reports

Two major update reports were sent to my University Supervisor during the course of the project, detailing aims, plans, problems and progress made. Scans of the original reports, as signed by my contractor Arjan Verweij, can be found in the corresponding files on the submitted CD.

Appendix H.1 1st Interim Report

1st Interim Report as written, dated: 30/07/2011

Appendix H.2 2nd Interim Report

1st Interim Report as written, dated: 09/11/2011

Appendix I - Industrial Project EE5 Project Plan

Project Progress and Reflection on Predictions/Projections

Shown below, is the final update (updated 09/11/11) of the constructed basic project plan, in the form of a Gantt chart. This chart was updated throughout the project, detailing the progress made in relation to that which was predicted. It can be seen, when comparing predictions (see **Appendix H.1**) that the times taken to complete each task were within an acceptable deviation from that which was expected. The project was also fully completed to the specified aims within the given period of employment.

Overall, I was very proud of the general progression of the project and the standard of work carried out, impressing my colleagues, on numerous occasions, as I had completed the work well within the expected time frame.

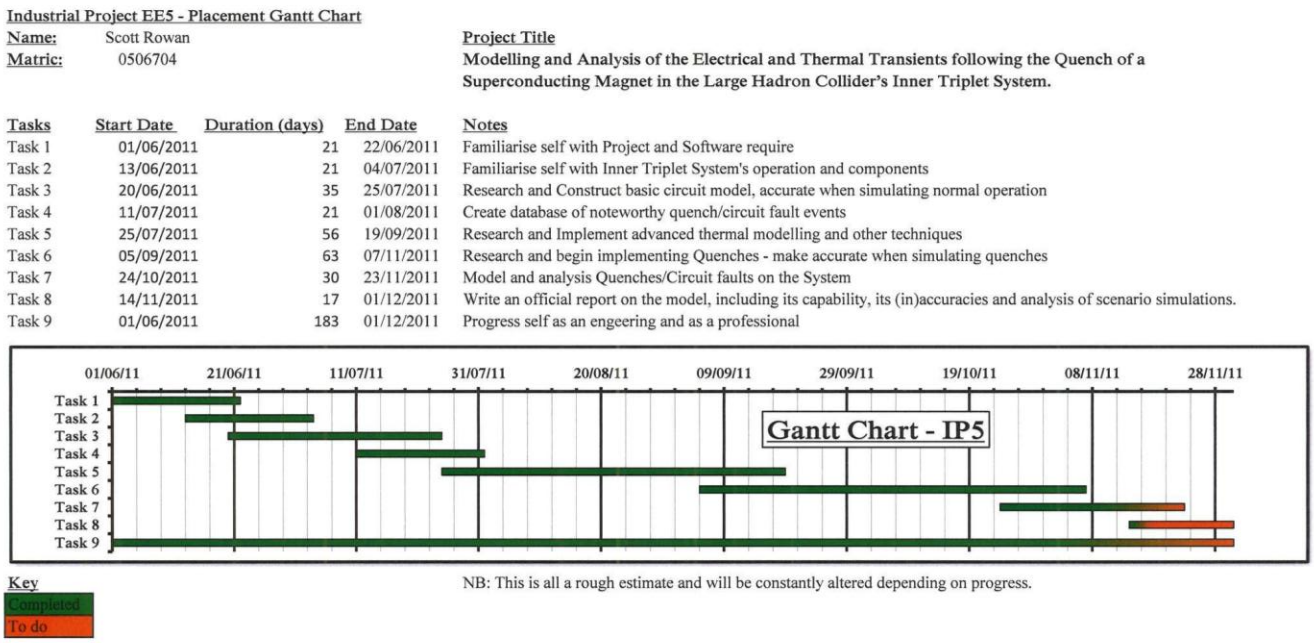
Industrial Project EE5 - Placement Gantt Chart

Name: Scott Rowan

Matric: 0506704

Project Title

Modelling and Analysis of the Electrical and Thermal Transients following the Quench of a Superconducting Magnet in the Large Hadron Collider's Inner Triplet System.

Tasks	Start Date	Duration (days)	End Date	Notes
Task 1	01/06/2011	21	22/06/2011	Familiarise self with Project and Software require
Task 2	13/06/2011	21	04/07/2011	Familiarise self with Inner Triplet System's operation and components
Task 3	20/06/2011	35	25/07/2011	Research and Construct basic circuit model, accurate when simulating normal operation
Task 4	11/07/2011	21	01/08/2011	Create database of noteworthy quench/circuit fault events
Task 5	25/07/2011	56	19/09/2011	Research and Implement advanced thermal modelling and other techniques
Task 6	05/09/2011	63	07/11/2011	Research and begin implementing Quenches - make accurate when simulating quenches
Task 7	24/10/2011	30	23/11/2011	Model and analysis Quenches/Circuit faults on the System
Task 8	14/11/2011	17	01/12/2011	Write an official report on the model, including its capability, its (in)accuracies and analysis of scenario simulations.
Task 9	01/06/2011	183	01/12/2011	Progress self as an engeering and as a professional

Key
Completed
To do

NB: This is all a rough estimate and will be constantly altered depending on progress.

Figure 36: Gantt chart showing the Project Plan and the progress made as of 09/11/11